Millennial-scale phase relationships between ice-core and Mediterranean marine records: insights from high-precision 40Ar/39Ar dating of the Green Tuff of Pantelleria, Sicily Strait

Stéphane Scaillet, Grazia Vita-Scaillet, Silvio G. Rotolo

Millennial-scale phase relationships between ice-core and Mediterranean marine records: insights from high-precision ^{40}Ar/^{39}Ar dating of the Green Tuff of Pantelleria, Sicily Strait

S. Scaillet, G. Vita-Scaillet

Institut des Sciences de la Terre d'Orléans (ISTO), INSU-CNRS, Université d'Orléans, 1A rue de la Férolerie, 45071 Orléans Cedex 2, France

S.G. Rotolo

Dip. Scienze della Terra e del Mare (DiSTeM), Università di Palermo, Via Archirafi 22, 90123 Palermo, Italy

Istituto Nazionale di Geofisica e Vulcanologia (INGV), Sezione di Palermo, Via U. La Malfa 153, 90146 Palermo, Italy

Corresponding author: S. Scaillet, Institut des Sciences de la Terre d'Orléans (ISTO), 1A rue de la Férolerie, 45071 Orléans Cedex 2, France (sscaille@cnrs-orleans.fr) (phone: + 33 2 38 25 53 80)

Highlights

• Revised $^{40}Ar/^{39}Ar$ age of the Green Tuff of Pantelleria is 44.1 ± 0.6 ka

• Revised orbital-tuning of deep-sea Y-6 tephra equivalent yields 42-44 ka

• Agreement between both estimates reconciles radiometric and orbital timescales

• First $^{40}Ar/^{39}Ar$ tie-point with near-millennial resolution in the marine record

Keywords

• Radioisotopic timescale, Green Tuff, Pantelleria, Tephrochronology, Ar/Ar dating

Abstract

With the advent of annually-resolved polar ice records extending back to 70 ka, marine and continental paleoclimate studies have now matured into a discipline where high-quality age control is essential for putting on an equal pace layer-counted timescale models and Late Quaternary sedimentary records. High-resolution U-Th dating of speleothem records and $^{40}Ar/^{39}Ar$ dating of globally recorded geomagnetic excursions have recently improved the time calibration of Quaternary archives, reflecting the cross-disciplinary effort made to synchronize the geologic record at the millennial scale. Yet, tie-points with such an absolute age control remain scarce for paleoclimatic time-series extending beyond the radiocarbon timescale, most notably in the marine record. Far-travelled tephra layers recorded both onland and offshore provide an alternative in such instance to synchronize continental and marine archives via high-resolution $^{40}Ar/^{39}Ar$ dating of the parent volcanic eruption. High-resolution $^{40}Ar/^{39}Ar$ data are reported herein for one such volcanic marker, the Green Tuff of Pantelleria and its Y-6 tephra equivalent recorded throughout the Central and Eastern Mediterranean. Published radiochronometric and $\delta^{18}O$ orbitally-tied ages for this marker horizon scatter widely from about 41 ka up to 56 ka. Our new $^{40}Ar/^{39}Ar$ age at 45.7 ± 1.0 ka (2σ) reveals that previous estimates are biased by more than their reported errors would suggest, including recent orbital tuning of marine records hosting the tephra bed that are reevaluated in the context of this study. This improved estimate enables potential phase lags and leads to be studied between deep-sea and terrestrial archives with unrivaled (near-millennial) $^{40}Ar/^{39}Ar$ precision in the marine record.

1. Introduction

Orbitally-tuned marine chronologies carry uncertainties inherent to global deep-sea $\delta^{18}O$ master curves to which they are tied (von Dobenek and Schmieder, 1999; Huybers and Wunsch, 2004). These derive from the choice in time lag relative to the target insolation curve and from phasing assumptions with the proxy carrying the climatic signal ($\delta^{18}O$ stratigraphy, organic carbon content, sea surface temperature, benthic/planktic biozones, sapropel events, sediment magnetic record, etc.). Tuning strategies also depend on starting tie-points used for recursive matching of proxy fluctuations to target orbital frequencies (e.g., Karner et al., 2002), with a precision of roughly a quarter of precessional cycle (~ 5 ka, Waelbroeck et al., 2008). They may be prone to loss in spectral power due to smearing artifacts (bioturbation, diagenesis, piston core deformation) that compromise phase-fitting relationships in the process of matching depositional time-series to their assumed orbital pacemaker. Lastly, erosion by bottom currents, discontinuous sedimentation, invasive mass flow by turbidites/slumping, and tectonic repetition/ablation may conspire to produce discontinuous or out-of-sequence records that cannot be directly matched with astrochronologic templates. Such complications may introduce systematic phase-tuning errors that add up back in time and may go unrecognized in progressively older archives.

Tephra deposits represent ideal control points for age modeling of deep-sea time-series because they can be isotopically dated by the $^{40}Ar/^{39}Ar$ technique independent of any orbital or continuum deposition assumption (Smith et al., 1996; van den Bogaard et al., 1999; Ton-That et al., 2001). In the central and eastern Mediterranean, recognition of such tephra layers and their correlation to known eruptive events is an area of active research for improving the tephrostratigraphy of marine and lacustrine sequences in a mid-latitudinal region where the climatic signal is amplified by marked seasonal effects and a semi-closed oceanic circulation (Hilgen et al., 1993; Paterne et al., 2008; Wulf et al., 2004, 2008; Turney et al., 2008; Zanchetta et al., 2008; Aksu et al., 2008). While recent progress has been achieved in dating

such tephras by ^{14}C bracketing (Siani et al., 2001, 2004; Lowe et al., 2007; Blockley et al., 2102), absolute age constraints remain relatively scarce for tephra beds lying beyond the reach of the radiocarbon timescale (Smith et al., 1996; van den Bogaard et al., 1999; Ton-That et al., 2001). As a result, Pleistocene tephras older than 20 ka are commonly dated by correlation with the marine δ^{18}O isotope stratigraphy (Keller et al., 1978; Thunell et al., 1979; Paterne et al., 1986, 1988, 2008) or multi-proxy phase-fitting insolation chronologies of orbitally-driven depositional sequences (e.g., Lourens, 2004; Piva et al., 2008), providing in such instances no independent control on orbitally-tuned age models.

With the emergence of annually-resolved polar ice records extending back to ca. 70 ka (Svensson et al., 2008; Austin and Hibbert, 2012), marine and continental paleoclimate studies have now matured into a discipline where high-quality age control is essential for putting on an equal pace layer-counted timescale models and Late Quaternary sedimentary records. While high-resolution U-Th and ^{40}Ar/^{39}Ar dating of globally recorded geomagnetic excursions (e.g., the Laschamp event) and speleothem records has consideraby improved the absolute time calibration of Quaternary archives (e.g., Singer et al., 2009; Genty et al., 2010; Vazquez and Lidzbarski, 2012), tie-points with near-millennial absolute age control remain crudely scarce for paleoclimatic time-series extending beyond the radiocarbon timescale, especially in the marine record.

Herein we report the result of a high resolution ^{40}Ar/^{39}Ar study of one such tie-point recognized as the Y-6 tephra layer throughout most of the Central and Eastern Mediterranean. Y-6 is important for paleoclimatic time-series spanning the last glacial cycle because it provides a unique tie-point at the lower limit of the radiocarbon timescale (~ 45 ka) where the precision of the ^{40}Ar/^{39}Ar technique outperforms the nominal accuracy of astrochronologic age models while narrowing the ± 1.2 ka b2k (before year AD 2000) resolution of layer-counted polar ice calendar ages in this time interval (Svensson et al., 2008). By working with near-millennial resolution in the marine record, this study reinforces the potential of high-

resolution $^{40}Ar/^{39}Ar$ tephrochronology for refining the constraining power of Late Quaternary tephra markers both as phase-fitting control points and long-range chronostratigraphic correlation tools.

2. The Green Tuff (GT) of Pantelleria and the Y-6 ash layer

Among the main tephra markers widely recognized in the central-eastern Mediterranean is the Late Pleistocene tephra bed Y-6, first named by Keller et al. (1978) after the foraminiferal biozone Y in which it occurs in the Ionian sea. Y-6 is referenced in the strategic tephra inventory reported by the extended INTIMATE event stratigraphy project (Blockley et al., 2012). The Y-6 tephra bed was first described in core logs RC9-191 and RC9-183 from the Ionian and Levantine seas (Keller et al., 1978; Fig. 1) with an assigned age of ca. 45 ka based on the biozone Y within Marine Isotope Stage (MIS) 3. The ash bed has since then been traced in different deep-sea cores, mostly throughout the Ionian sea (Negri et al., 1999), in lacustrine series in Albania (Vogel et al., 2010; Sulpizio et al., 2010), and at distal locations as far afield as the Dodecanese more than 1200 km away from the inferred source (Calanchi et al., 1998; Narcisi and Vezzoli, 1999; Margari et al., 2007; Fig. 1).

As for other far-travelled tephras, the wide dispersal of the Y-6 layer is diagnostic of a high-energy eruption associated with caldera-collapse and emission of a Plinian convective plume. The Y-6 layer stands apart other Mediterranean tephras by its characteristic peralkaline signature differing from the trachyphonolite, high-K calkaline, or rhyodacite composition shared by many volcanic centres in mainland Italy and the Aegean arc. This distinctive composition can be unequivocally traced to the volcanic island of Pantelleria (Keller et al., 1978), the only peralkaline centre active in the Mediterranean since the Middle Pleistocene (450 ka to present), making this and older Pantellerian markers particularly valuable for long-distance tephrostratigraphic correlations (e.g., Caron et al., 2010).

In spite of very favourable exposure of its inferred onland equivalent (the Green Tuff of Pantelleria island, Sicily Strait), the absolute age of Y-6 remains loosely constrained, largely undermining its potential as a basin-wide chronostratigraphic tie-point. The age of the Y-6 tephra has long been correlated with the Green Tuff (GT) associated with the last large-magnitude eruption of Pantelleria. Early investigations by bulk K-Ar dating of anorthoclase crystals from proximal GT deposits by Cornette et al. (1983), Mahood and Hildreth (1986), and Civetta et al. (1988), yielded ages scattering from 46.9 ± 3.4 ka to 55 ± 8 ka (2σ, cf. Table 5). Added to this scatter, the contraining power of these data appears suspect due to the inability of K-Ar ages to resolve xenocrystic contamination and/or the presence of excess argon (e.g., Lo Bello et al., 1987; van den Bogaard et al., 1987; Gansecki et al., 1996; Scaillet et al., 2008, 2011). Also, these data were derived from total fusion of very large (2-15 g) feldspar aliquots and thus may be prone to uncomplete argon extraction and biased apparent ages (McDowell, 1983). An unpublished $^{40}Ar/^{39}Ar$ study of the GT was undertaken a decade ago by Ton-That (2001) on the same samples originally dated by Mahood and Hildreth (1986), yielding similar ages in the range 52.4 ± 5.8 ka to 45.4 ± 2.1 ka (2σ, recalculated using updated decay constants and monitors values following Renne et al., 2010, 2011).

As a result of their internal and between-sample scatter, moderate confidence has been assigned so far to these ages, leaving the early estimate of ~ 45 ka of Keller et al. (1978) widely accepted for its putative Y-6 distal equivalent (e.g., Narcisi and Vezzoli, 1999). One problem with such estimate is that logging details ($\delta^{18}O$ stratigraphy, in-core tephra depth) were not fully disclosed to properly assess the accuracy of the supporting age model. As reviewed further below, integration of existing radiometric data with more recent $\delta^{18}O$, ^{14}C, and biozone-tied stratigraphic estimates still conveys a somewhat blurred picture of the actual age-constraining power of Y-6. This situation is reflected by the use of widely disparate age estimates in the recent tephrostatrigraphic literature reporting Y-6 (Sulpizio et al., 2010; Vogel et al., 2010; Caron et al., 2010; Tamburrino, 2008), often without stated justification for preferring one age over another.

The scope for improving the radiometric estimate of the GT eruption is therefore twofold. First, to provide a direct and more robust calibration of multi-proxy paleoclimatic cores recording Y-6 (e.g., Tamburrino et al., 2012). Next, to keep pace with the ever improving precision of Late-Pleistocene paleoclimatic reconstructions spanning the last glacial cycle in this particular area (e.g., Lourens, 2004; Sprovieri et al., 2012). In the Y-6 case, it is a rare circumstance that a distal tephra marker may be so unequivocally matched with its proximal equivalent, and the obvious step forward is to apply high-resolution $^{40}Ar/^{39}Ar$ dating to the GT proper by taking advantage of its excellent exposure and state of preservation at Pantelleria, as we describe below.

3. Structure and geochemical fingerprinting of the GT

The GT is the product of a large-magnitude eruption associated with the collapse of the ~ 30 km² "Cinque Denti" caldera of Pantelleria (Mahood and Hildreth, 1986). As with many other distal tephras (e.g., Thunell et al., 1979), the outboard marine Y-6 deposit corresponds to a co-ignimbrite ash-fall and distal fallout probably at least as important in volume as the GT ignimbrite sheet itself (~ 4-7 km³ dense rock equivalent, DRE; Wolff and Wright, 1981; Mahood and Hildreth, 1986; Civetta et al., 1988). An accurate volume estimate has not been attempted yet. The minimum dispersal area for the Y-6 tephra (7×10^5 km²) coupled with the cm-thickness of its putative ash bed equivalent ML-5 at Lesvos has suggested a bulk ash volume around 25 km³ (10 km³ DRE, Margari et al., 2007), second in rank but similar in importance to other large-magnitude eruptions in the Aegean sea (Z-2 = Minoan, Y-2 = Cape Riva).

Onland, the GT consists of several layered members reflecting fluctuations in eruptive dynamics, magma temperature, and transport energy during eruption (Orsi and Sheridan, 1984; Fig. 2). An extensive field and lithofacies survey of the GT zoneography has been

reported recently by Williams (2010) to whom the reader is referred for a full account of the depositional mechanisms envisioned for its formation. Compositionally, the GT erupted as a compound unit grading from pantellerite at the base into comenditic trachyte at the top, indicating progressive withdrawal from a zoned magma chamber (Mahood and Hildreth, 1986; Civetta et al., 1988). Despite its marked lithofacies variations, the bulk (~ 90 %) of the GT is thought to represent a single pyroclastic density current that was tapping increasingly crystal-rich magmas through the eruption (Williams, 2010). The most complete sequence is found in the NE of the island, between the lake Specchio di Venere and Cala Cinque Denti (Fig. 1). It consists of at least five subfacies (or members), from base to top:

(A)   A 60-70 cm thick and poorly sorted Plinian fall of evolved pantellerite composition.

(B)   A 40-50 cm thick unwelded and fines-rich pumice flow with a slightly more evolved pantellerite composition.

(C)   A 70 cm thick densely welded facies, slightly less evolved compositionally than the lower members and lined by a characteristic basal vitrophyre, 10-15 cm thick.

(D)   A 1 m thick, conspicuously green-coloured, strongly welded massive layer ubiquituous throughout the island and chemically similar to the underlying Member C.

(E)   A discontinuous crystal-rich upper member with a distinctively less peralkaline (trachytic) composition.

Mineralogical and depositional features are detailed for each member in Tables 3 and 4. Bulk (glass) compositions are plotted in Fig. 3 and tabulated in Table 2. The phenocryst content (vesicle-free) is $\leq$ 10 vol.% for members A-B and increases to 15 vol.% (member D) and 30 vol.% (Member E). The compositional grading from pantellerite (A) to trachyte (E) is mirrored by variations in differentiation-index rare-earth elements, notably Zr that decreases from ~ 1900 to 300 ppm. A parallel decrease in peralkalinity index (PI = $(Na_2O+K_2O)/Al_2O_3$ molar) is observed through the sequence: PI = 1.7 (A), 1.80 (B), 1.7 (C), 1.3 (D), 1.0 (E), a

trend exacerbated in the topmost member by feldspar fractionation due to fines loss (Rotolo et al., 2013)

The GT compositional zoning is important to consider for accurate identification of distal equivalents which may represent a mixture between the pantellerite/trachyte endmembers during long-range dispersal and deposition. Orsi and Sheridan (1984) suggested that the distal outboard component originates from the early fines-depleted Plinian fall member (basal Member A). They noted however that the volumetrically dominant, crystal-rich, terminal ash flow units (correlative to units D and E above) bear evidence for a significant windblown co-ignimbrite ash cloud (see also Wolff and Wright, 1981). We infer that Member D along with the volumetrically subsidiary Member E represent the most likely source for the distal tephra layer Y-6 and correlatives. This is corroborated by glass shard analyses reported for at least three distal occurences (Lesvos island: Margari et al., 2007; Ionian sea: Tamburrino et al., 2012; Orhid Lake: Vogel et al., 2010) showing a mixed pantellerite/trachyte composition that match the GT pantellerite-trachyte bimodality with a REE signature sympathetic to the proximal deposits (Figs. 3, 4).

4. ^{40}Ar/^{39}Ar geochronology and results

Representative ^{40}Ar/^{39}Ar samples were selected from two porphyritic GT facies from Member C exposed near Cala Cinque Denti (Figs. 1, 2). All samples come from fresh, strongly (dark-green) to moderately (pale-green) welded ash flows with crystal contents up to 5-10 vol.% dominated by 2-5 mm-sized euhedral anorthoclase with subordinate phenocrysts of clinopyroxene + aenigmatite set in a weakly to moderately devitrified matrix. Ilmenite ± fayalite ± quartz occur as accessory phases with sparse amphibole microphenocrysts due to vapour-phase crystallization. Sample PAN 0657 is from the thin basal vitrophyre lining the lithic- and fiamme-rich lower portion of Member C at the contact with the caldera wall exposed at Cala Cinque Denti, directly above pre-caldera ignimbrite Z (~ 85 ka, Rotolo et al.,

2013). Sample PAN 0674 is from the overlying welded facies C proper, about 100 m hinterland from PAN 0657.

Samples were irradiated along with the flux monitors ACR-2 and TCR-2 in the Cd-lined β-1 slot of the Osiris nuclear facility (CEA, Saclay) with a fast neutron fluence of 4.1×10^{16} n/cm^2 or 2.7×10^{17} n/cm^2, following procedures and correction factors detailed in Scaillet et al. (2008, 2011) and in supplemental file S1. Complete age data are tabulated in supplemental Table S1 and summarized in Table 1. Our ages are tied to the Fish Canyon Tuff (FCT) sanidine via the monitor intercalibration data set of Renne et al. (2010, 2011) who recently determined an U/Pb-intercalibrated age of 28.294 ± 0.072 My for FCT (2σ). This age is four precession cycles (~ 21 ka) older than (but within error of) the calibration of Kuiper et al. (2008) for this monitor based on astrochronologic tuning of tephra-hosting Upper Miocene beds in Morocco (28.201 ± 0.046 Ma, no confidence level quoted).

The relative difference of 0.3 % between both calibrations translates into a trivial delta-age of 0.14 ka in the time interval pertinent to this study. Such a difference is not resolvable within our analytical uncertainties and is not (yet) critical in terms absolute time calibration of the Green Tuff deposition. Recent astrochronologic tuning of FCT against an other orbitally-tied Late Miocene tephra bed in Crete revealed a similar mismatch with the U/Pb calibration by returning FCT @ 28.172 ± 0.028 My (2σ; Rivera et al., 2011). However, exhaustive calibration of instrumental performances casts some doubts as to whether such a ± 0.1 % accuracy (i.e., 2σ full external error) can be reliably obtained from multi-collection ^{40}Ar/^{39}Ar data in the absence of very closely monitored short-term intercollector mass-bias (Coble et al., 2011). Independent astronomic calibration of FCT at a significantly younger age of 27.89 Ma by Westerhold et al. (2012) illustrates that the debate around its absolute age by orbital tuning is not going to settle down quickly. We just note here that the choice of either calibration (radioisotopic or astrochronologic) is inconsequential in terms of ^{40}Ar/^{39}Ar dating of Pleistocene events, and adopt the U/Pb intercalibrated values of Renne et al. (2011) to avoid

the circularity of using an orbitally-tied monitor's model age to provide a reference point for other orbitally-tuned climatic time-series.

PAN 0674 was analyzed in duplicate (PAN 0674bis) and a total of 73 individual ages were extracted from the different samples. These yielded internally consistent results with weighted mean ages of 42.8 ± 1.2 ka (PAN 0657, *MSWD* = 0.76 ∈ [0.45-1.72]), 45.4 ± 1.0 ka (PAN 0674; *MSWD* = 1.44 ∈ [0.60-1.48]) and 44.7 ± 1.0 ka (PAN 0674bis, *MSWD* = 0.34 ∈ [0.61-1.47]) (total weighted averages; *MSWD* = Mean Square Weighted Deviation; 95 % fiducial interval of *MSWD* in square brackets, cf. Scaillet et al., 2011). The gas fractions evolved at low temperature for sample PAN 0674 yielded slightly older ages possibly reflecting surficial contamination with excess argon, a fact already noted for other young anorthoclases from Pantelleria (Scaillet et al., 2011). These individual ages do not detract, however, from their respective internal mean at 2σ. The mean ages of PAN 0657 and PAN 0674 are just resolved at 2σ, while PAN 0674bis is fully consistent with its companion aliquot PAN 0674. The anorthoclase phenocrysts from the glassy vitrophyre (PAN 0657) shows slightly more contaminated (i.e., atmospheric-like) ^{40}Ar/^{36}Ar ratios (Table S1), probably as a result of enhanced air entrapment during rapid high-T agglutination of melt + crystal particles and rapid quenching at the ground.

PAN 0657 and PAN 0674 define internally consistent, but mutually discordant, isochron ages at 42.5 ± 2.0 ka (*MSWD* = 0.81 ∈ [0.44-1.75]) and 47.4 ± 1.6 ka (*MSWD* = 1.13 ∈ [0.60-1.49]) respectively. These are not distinct from their corresponding total-gas ages. PAN 0674bis yielded an internally concordant isochron age of 46.2 ± 2.5 ka ka, with a *MSWD* score of 0.29 ∉ [0.60-1.48] flagging some underscatter possibly signaling overestimation of individual errors. The intercept ^{40}Ar/^{36}Ar ratio is indistinguishable from the atmospheric composition in vitrophyre PAN 0657 (296.1 ± 3.3), and slightly sub-atmospheric for the less contaminated welded facies PAN 0674 (291.0 ± 2.8) and PAN 0674bis (291.2 ± 6.4).

5. Discussion

5.1 Comparison with prior radiometric data

Our ^{40}Ar/^{39}Ar ages are significantly younger (by up to 10 %) and much grouped than previous K-Ar and ^{40}Ar/^{39}Ar determinations on equivalent GT facies (Tables 1 and 5). Mahood and Hildreth (1986) speculated that the older (though concordant) K-Ar age they obtained for the trachytic top (GTP-233 = 50 ± 9 ka, 6 km SW of Cala Cinque Denti) relative to the basal age of the sequence (GTP-19 = 44.5 ± 6.2 ka, 3 km NW of Cala Cinque Denti) could reflect excess ^{40}Ar derived from undegassed magma tapped from deeper into the zoned magma chamber, artificially raising the age of the top member GTP-233. Ton-That (2001) data reproduce a similar trend with 45.2 ± 1.9 ka (GTP-19, base) < 47.7 ± 1.5 ka (GTP-226) < 52.5 ± 5.8 ka (GTP-233, top). Our own data for Member C appear to mimic a similar trend with an apparent top-base gradient of 2.3 ± 1.4 ka (Table 1), although all samples originate from the same flow unit (and parent magma). This raises the question whether such a trend is significant and symptomatic of (i) pre-eruptive ^{40}Ar heterogneities inherited from chamber-scale volatile zoning, or (ii) a top-to-base syn-depositional effect on trapped ^{40}Ar/^{36}Ar.

We hardly see any reason why the anorthoclases dated here or in previous studies could record pre-eruptive volatile heterogeneities or some chamber-scale sectorial zoning/stratification with variable dissolved ^{40}Ar. This would require very fortuitous, hence quite unlikely, preservation of magmatic gradients despite the highly dispersive forces attending magma withdrawal and subsequent airborne deposition (especially in our case involving no apparent geochemical zonation in the same depositional member). Separate ^{40}Ar/^{39}Ar analysis of anorthoclase crystals purposely selected for their high content in melt inclusions (MI) already showed that these are not resolvable in age from the other (MI-poor) specimens (Ton-That, 2001), ruling out the presence of significant excess ^{40}Ar in the parent melt. Selective contamination with accidental xenocrysts retaining pre-eruptive ages is also

unlikely to explain the age gradient as this would have typically resulted in erratic age distributions with multiple scattered modes (e.g., Scaillet et al., 2011), none of which occur here (Fig. 5).

The mechanisms of air ingestion, mechanical trapping, and dissolution in a welding ash fall or flow with desorption back into the atmosphere upon devitrification and hydration are poorly quantified phenomena that are potentially conducive to $^{40}Ar/^{36}Ar$ mass-fractionation. Our data are qualitatively consistent with the expectation that glassy specimens collected near the base of an airfall or pyroclastic unit should contain larger proportions of dissolved atmospheric Ar mechanically trapped during agglutination and welding at the ground (Marvin et al., 1970). However, fractionation of the $^{40}Ar/^{36}Ar$ trapped along with age-aliasing effects is unlikely to have occurred in such circumstances because cooling of the 10 cm-thick basal vitrophyre PAN 0657 must have proceeded via a quenching process fast enough to inhibit significant melt-crystal diffusional exchange with mass-fractionation (and preferential ^{36}Ar uptake) in anorthoclase.

This is borne out by the higher atmospheric content coupled with the atmospheric-like intercept observed for the anorthoclases of this facies (296.1 ± 3.3, Table 1), ruling out significant mass-dependent uptake fractionation during basal cooling. Likewise, the m-thickness of Member C at the PAN 0674 sampling site is not significant enough to have delayed cooling to the extent characteristic of much thicker (> 10 m) obsidian flow-domes. $^{40}Ar/^{36}Ar$ fractionation effects reported in slowly-cooled (solid-state) obsidian flows are documented in the metastable melt/glass phase only. They have not been found to affect the enclosed anorthoclase (Morgan et al., 2009). Based on thermal-diffusion modeling of thin ignimbrites sheets (Spell et al., 2001; Wallace et al., 2003), such diffusional effects are expected to rapidly fade away in mm-sized pre-eruptive crystals during subsolidus post-depositional cooling, even in the case of the welded interior of Member C (PAN 0674 and PAN 0674bis) that probably cooled down to 200 °C in less than ~ 1-2 months or so. Any

associated age-aliasing effect must have only peripherally affected the $^{40}Ar/^{39}Ar$ age of these crystals. This conclusion is strengthened by the fact the isochron data from these samples are mainly derived from the high-T (fusion) step that reflects degassing from the crystal interiors (the first low-T step was generally discarded to minimize the surface-bound atmospheric component, cf. supplemental file S1).

When regressed in an isochron plot, a slight difference in trapped $^{40}Ar/^{36}Ar$ ratio is barely apparent between the vitrophyre and the welded facies (296 ± 3 vs. 291 ± 3, Table 1), failing to resolve any distinct mass-fractionation effect according to the sample position. Actually, the three samples collectively define an internally-consistent isochron with a slightly sub-atmospheric ratio of $(^{40}Ar/^{36}Ar)_{trapped} = 292.7 \pm 2.0$ and an age of 45.7 ± 1.0 ka ($MSWD = 0.90$ $\in [0.74\text{-}1.29]$, $N = 73$) that is indistinguishable from their lumped integrated age at 44.4 ± 0.6 ka (Table 1, Fig. 6). Geometrically, any homogeneous fractionation during trapping of the $^{40}Ar/^{36}Ar$ ratio would cause the pooled isochron to be tilted around the purely radiogenic $^{39}Ar/^{40}Ar$ intercept, ideally projecting to the (common) fractionated $^{36}Ar/^{40}Ar$ intercept while leaving unaffected the isochron age.

The higher precision of our data uncovers a statistically significant difference of ca. 3 ka relative to the data of Ton-That (2001). Regression of all her analyses in an isochron plot produces an isochron with an $^{40}Ar/^{36}Ar$ intercept indistinguishable from our sample suite (293.7 ± 2.8), yet with a significantly older age of 48.8 ± 2.0 ka ($MSWD = 0.97 \in [0.79\text{-}1.23]$, $N = 110$; Table 5). Clearly, this ~ 3 ka age difference cannot be explained by selective $^{40}Ar/^{36}Ar$ fractionation among the different samples as this effect is automatically accounted for by the isochron formalism. A more likely explanation is that the difference derives from unaccounted variations in the $(^{40}Ar/^{39}Ar)_K$ production ratio among the facilities used for irradiation. Geometrically, a variation in the $(^{40}Ar/^{39}Ar)_K$ correction factor does the opposite of the fractionation effect by tilting the isochron slope about the $^{40}Ar/^{36}Ar$ intercept (acting as a pivot immune from any error in the $^{40}Ar_K$ correction). Although Cd-shielding was applied in

both cases to reduce ^{40}Ar production from ^{40}K, close monitoring of the shielding factor showed this not to be 100 % efficient at Osiris with a non-vanishing $(^{40}Ar/^{39}Ar)_K$ ratio of 4.6 ($\pm$ 2.0) $\times$ 10^{-3}. Ton-That (2001) applied a significantly lower correction ratio of 8.6×10^{-4} (no error quoted) for the CLICIT position of the Triga reactor at OSU. This ratio was not measured directly but retrieved from literature data (B. Singer, e-communication, 2011). Published data from CLICIT indicate that $(^{40}Ar/^{39}Ar)_K$ may vary there between 3.97×10^{-3} and 1.40×10^{-4} with an average at 1.1 ($\pm$ 1.2) $\times$ 10^{-3} (M.S.E. of observed scatter; Renne et al., 1998), pointing to variable shielding efficiency.

Two options thus apply. Either one of the correction factors applied is flawed, or both datasets are corrupted to an extent underestimated by both laboratories. Although we have no reason to question the value used by Ton-That (2001), we note that our aliquot 06-074bis irradiated for only 2 min - virtually eliminating any bias in the $(^{40}Ar/^{39}Ar)_K$ correction - yielded an age identical to the companion aliquot PAN 0674 irradiated with a much higher fluence. Had the $(^{40}Ar/^{39}Ar)_K$ ratio been substantially overestimated, a significantly different age would have resulted for both replicates, from which we feel confident in considering our $(^{40}Ar/^{39}Ar)_K$ value and pooled $^{40}Ar/^{39}Ar$ age estimate quite robust. Sub-atmospheric $^{40}Ar/^{36}Ar$ isochron intercepts are commonly (but improperly) traced to a wrong $(^{40}Ar/^{39}Ar)_K$ correction which, we have seen, increasingly corrupts the fractions plotting progressively away from the $^{36}Ar/^{40}Ar$ intercept along the isochron, leaving unaltered the trapped $^{40}Ar/^{36}Ar$ end-member itself. We argue here that the ^{40}K interference on ^{40}Ar has been properly accounted for, that the regressed sub-atmospheric ratio is not an artifact of the irradiation procedure, and that the isochron-intercept age is not altered by the $^{40}Ar/^{36}Ar$ fractionation implied. The latter does indicate, however, that the trapped component is affected to an extent sufficient to potentially bias the isotopic composition of low-T (surface-bound) retentive sites. Such an effect has been efficiently minimized by our predegassing (two-step) procedure, as testified by the remarkably enriched radiogenic signature obtained for a sample that young with only ~ 5 wt%

K (Fig. 6). Clearly, undue recognition of the fact may be very detrimental in more routine work on similarly young samples if these are not pre-degassed via a dedicated protocol.

In summary, we elect the value of 44.4 ± 0.6 ka (45.7 ± 1.0 ka, 2σ, allowing for a slight age-aliasing fractionation) as the best current estimate of the $^{40}Ar/^{39}Ar$ age of the GT eruption and the primary Y-6 layer deposition. This estimate includes the errors from the decay constants and monitor's age for proper comparison with non radio-isotopic (calendar) timescales and represents a substantial improvement over previous K-Ar and $^{40}Ar/^{39}Ar$ determinations both in terms of absolute age control and internal consistency.

5.2 Comparison with $\delta^{18}O$-tied stratigraphic age estimates for Y-6

The early estimate of ~ 45 ka for Y-6 in core RC9-191 by Keller et al. (1978) was originally tied to the astronomical calibration of Emiliani and Shackleton (1974), although no depth-age model was provided then in support of the estimate. This estimate was later refined to 44.6-44.1 ka (interpolated between MIS 3.13-3.3) by Kraml (1997) in core M25/4-13 in the Ionian Sea (Schmiedl et al., 1998) based on the subsequent astronomical calibration of Martinson et al. (1987). From recent age modelling of a distal tephrostratigraphic sequence on Lesvos (Greece) combining AMS ^{14}C dates with a high-resolution pollen stratigraphy tied to the GISP2 timescale, Margari et al. (2007) re-evaluated the age of Y-6 at 53.6 ± 11.4 ka (2σ), although the correlation with Y-6 is disputed by Vogel et al. (2010) on the basis of significantly lower contents in SiO_2 and FeO_t.

AMS ^{14}C age-bracketing from a biogenic carbonate ooze underlying the proximal GT volcanoclastic facies cored off Pantelleria suggests an age > 43 ± 2 ka cal BP, based on the U-series calibration of Bard et al. (2004) and the GISP timescale (Anastasakis and Pe-Piper, 2006). Faunal attribution of the planktonic foraminiferal assemblage of the hemipelagic marl underlying this volcaniclastic level places the GT in biozone MNN 21b at this coring location

(Anastasakis and Pe-Piper, 2006), implying an age younger than the MNN 21a/b boundary (50 ka, Lourens, 2004). However, the base of the volcaniclastic succession appears erosional at this site and geochemical evidence indicates that the base of the sequence may consist of two different volcaniclastic units. While the association of peralkaline glass shards (PI = 1.54) with aenigmatite in the upper 26.0 - 26.7 m depth interval is compatible with the mineralogy and composition of the GT, an abrupt decrease of the glass peralkaline index to PI = 1.22 can be noted between 27.1 – 27.5 m. The 27.10 m depth discontinuity is also marked by the occurence of a 61 mol.% An plagioclase incompatible with the pantellerite composition of the GT. A possible onland equivalent may be the trachytic ignimbrite P (123 ka, Rotolo et al., 2013) or the trachy-comenditic ignimbrite Z (85 ka, *ibid*.), suggesting that the bottom of the sequence may actually consist of two different volcaniclastic units.

In core M25/4-12 (Ionian sea; Negri et al., 1999), the Y-6 tephra layer is assigned to MIS 3.2 by Anastasakis and Pe-Piper (2006), implying an age around 48 ka based on the Greenland ice chronology (Shackleton et al., 2004). The exact in-core depth position of Y-6 was not published by the original authors (and neither could be specified to us on request; A. Negri, e-mail communication, 2011). This is reported by Kraml (1997) to occur at 208 cm (depth from bottom sea floor) from which this author derived a significantly younger estimate of 41.6 ka (tuned to SPECMAP).

The last tuned age for Y-6 comes from the higher resolution record of ODP leg 160 site 963A cored off south-western Sicily (Emeis et al., 1996) and recently revised by Tamburrino (2008), Tamburrino et al. (2012), and Sprovieri et al. (2012). An age model based on visual matching of benthic $\delta^{18}O$ wiggles (and spikes in *G. ruber* abundance) with 17 Greenland Interstadials (GI) of the NGRIP record was established using the GICC05 timescale of Svensson et al. (2006, 2008) for the interval 20-42 ky, and the ss09sea chronology for the interval 42-65 ka (Sprovieri et al., 2012). The age interpolated through the GI tie-points (including two AMS ^{14}C foram dates) returns a value of 42.5 ka for Y-6 (Tamburrino, 2008).

An identical age of 42.5 ka is also claimed for Y-6 in the same core based on yet another age model tied to SPECMAP (Tamburrino et al., 2012; Table 5) using the isotope stratigraphy and quantitative eco-biostratigraphy of Incarbona et al. (2009).

A summary sketch of the $\delta^{18}O$-tied and NGRIP peak-matched calibration of the Y-6 ash layer is provided in Figs. 7 and 8 and listed in Table 5. In this figure, the benthic $\delta^{18}O$ profiles of the Ionian Meteor piston cores were retuned according to the MIS tie-points of the original age model of Schmiedl et al. (1998) for core M25/4-13, and the sapropel events S1 through S10 for M25/4-12 (as tabulated in Negri et al., 1999, and calibrated according to Lourens, 2004), plus some additional points hand-tied to the SPECMAP template. Core ODP-160-963A was retuned from a 5-point smoothed $\delta^{18}O$ profile hand-tied to the higher resolution $\delta^{18}O$-benthic stack LR04 (Lisiecki and Raymo, 2005) by pattern-matching of a composite (benthic + planktic) foram record from Howell et al. (1998; unpublished data courtesy of A. Incarbona, e-communication, 2012).

These revised calibrations return a consistent estimate at 42.2-42.5 ka for Y-6 in both Meteor cores (Figs. 7 and 8; Table 5). This is almost coincident with Tamburrino et al. (2012) estimate, although no particular effort was made to integrate both records simultaneously. A slightly older estimate at 44.7 ka is derived from the higher resolution core ODP-160-963A calibrated against LR04 (vs. 42.5 ka by Tamburrino et al., 2012, tied to SPECMAP). Such ± 2 ka departure from either Kraml (1997, core M25/4-13) or Tamburrino et al. (2012, core ODP-160-963A) is not surprising. This merely reflects the (probably underestimated) magnitude of the error involved in such an exercise given (i) the assumed linear interpolation, (ii) the moderate resolution of both Meteor cores, and (iii) the fact that Y-6 occurs in a MIS interval featuring the most subdued $\delta^{18}O$ profile across the last glacial cycle (hence for which it is difficult to pick up diagnostic $\delta^{18}O$ wiggles that can be unambiguously tied to the SPECMAP or LR04 templates).

Basically, the age models derived in the same core by Tamburrino et al. (2012) and Sprovieri et al. (2012) differ in that the first is based on long-term orbital oscillations, the second on sub-orbital climatic frequencies, i.e. at low and high-temporal resolution, respectively. As discussed further above, visual matching to either one or the other model age is inherently subjective. Alternative calibration of the GT against the original age model of Tamburrino et al. (2012) tied to NGRIP returns a visually-matched estimate at 45 ± 1 ka. This underscores both the convergence of hand-tied estimates around ~ 45 ka but, more importantly, the variability inherent to interpolating across different age models in the same record. Alternative estimates falling apart by more than 2 or 3 ka can result depending on which model is selected, the error involved being quantifiable only through high-resolution $^{40}Ar/^{39}Ar$ dating as done here.

We conclude that the error carried over by the revised times-series estimates is likely of the order of ± 3 ka (Fig. 8), and that these appear reasonably well grouped around 42-44 ka considering the simplification made in linearly interpolating between bracketing tie-points widely apart across MIS 3. Such estimates are conspicuously younger than previous K-Ar and $^{40}Ar/^{39}Ar$ ages for the GT (47-49 ka), including existing ^{14}C, orbitally, or eco-biostratigraphy-tied estimates derived from more distal records that lack, however, the necessary resolution to permit a meaningful comparison. Our revised $^{40}Ar/^{39}Ar$ estimate at 44-45 ka appears fairly consistent with the revised $\delta^{18}O$-tied chronostratigraphy of this study (especially against LR04 in core ODP-160-963A), reconciling much - if not all - of the disparity prevailing so far with previous radiometric determinations. Incidentally, the new $^{40}Ar/^{39}Ar$ age estimate lends support to the conclusion by Vogel et al. (2010) that the peralkaline tephra M5 recognized at Lesvos by Margari et al. (2007) is more probably correlated with the P-11 Mediterranean tephra layer (Paterne et al., 2008) than with the GT proper.

5.3 Millennial-scale phase relationships between ice-core and Mediterranean marine records?

Recent marine pollen records suggest that vegetation changes in south-western Europe during the last glacial cycle were synchronous with rapid sea-surface temperature variations closely matching the millennial-scale variability documented in Greenland ice cores through the Dansgaard/Oeschger (D/O) cycles (e.g., Combourieu Nebout et al., 2002, and references therein). The existence of specific D/O cycles across much the northern hemisphere is suggested by the presence of distinct Heinrich layers signaled by lithological (ice-rafted debris) and coeval biostratigraphical markers in North Atlantic and Western Mediterranean deep-sea cores (Cacho et al., 1999; Sierro et al., 2005; Allen et al., 1999; Sprovieri et al., 2012). Close pattern-matching of secular $\delta^{18}O$ trends recorded in Mediterranean planktonic forams and polar ice has suggested that the short-lived D/O warming events were homogeneously recorded across North Atlantic and the Mediterranean as a consequence of North Atlantic polar transients driven by major shifts in the northern hemisphere circulation (Fletcher et al., 2010).

Our $^{40}Ar/^{39}Ar$ age estimate basically supports, and substantially refines, tuning to global benthic stacks that tie Y-6 to MIS 3.13 at ca. 44-45 ka. On the other hand, the recognition of the Y-6 tephra in a high-resolution record (ODP 160-963) bearing evidence of high-frequency D/O-like cycles in the 20-60 ka interval provides a rare opportunity where the three chronologies (orbital, layer counting, and radiochronology) can be simultaneously compared. With a sampling frequency about twice to five times greater than other cores, the data from core ODP 160-963 represent a qualitative improvement with near-millennial resolution, potentially allowing phase relationships to be investigated relative to the Greenland timescale (Sprovieri et al., 2012; Tamburrino et al., 2012). The calibration of Tamburrino (2008) and Sprovieri et al. (2012, Fig. 7) essentially assumes (1) one-to-one correlation between Greenland D/O cycles and the $\delta^{18}O$ (and foram abundance) spikes identified in core ODP-160-963A; and (2) no time lag in the expression of the millennial-scale climate variability in both archives. This approach was justified by the strong link allegedly established by previous

studies between the $\delta^{18}O$ proxy in NGRIP and Mediterranean paleoceanographic time-series (Sprovieri et al., 2012).

The success of the ice-core calibration has fostered the belief that the D/O warming events were near-global in extent (van Andel, 2005), but assuming a zero phase lag in the transmission of North Atlantic climatic events through the Mediterranean marine record is a conceptual step that remains contentious (cf. Blaauw, 2012). This is especially so for marine time-series recorded at (or beyond) the limit of the radiocarbon technique, hence for which there is scarce (if any) independent radiochronologic control to support peak-to-peak matching of high-frequency $\delta^{18}O$ marine shifts with target D/O events. Recent studies (Genty et al., 2010) have documented differences in U-Th dated high-resolution records between continental areas under strong Atlantic influence (Villars cave, south-western France) and continental or marine sites further South and East (Alboran Sea; Monticchio varved sequence, southern Italy). Such results highlight differences in the individual expression of D/O events and the difficulty of synchronizing climatic proxies modulated by up to 1.5 ka regional phase lags between precession-dominated (Mediterranean) and mainly obliquity-dominated (middle latitudinal Atlantic) climatic systems.

The nominal 2.5 ± 0.6 ka age difference between our $^{40}Ar/^{39}Ar$ age and the 42.5 ka NGRIP-tied calibration of Tamburrino (2008) and Sprovieri et al. (2012) may be a reflection of this effect, potentially implying a phase shift of one D/O cycle length to align both records (Fig. 7). However, a more critical evaluation of potential D/O events in core ODP-160-963A is warranted before such a difference can be considered diagnostic of a true phase lag. Peak-to-peak matching by visual identification is subjective and prone to miscalibration if the matched time-series are just sharing similar spectral moments rather than true common events (Wunsch, 2006). Blaauw (2012) illustrates a synthetic example where two time-series tuned by assuming covariance of the signal correlation (while actually they are uncorrelated) provide a much better visual match than the one apparent in Fig. 7. As emphasized by this

author, tuned peaks are less reliable than uniquely identified tephra layers and should not be given the same chronological status. At present, it remains uncertain whether our $^{40}Ar/^{39}Ar$ age is reflecting a true phase lag or if the high-frequency $\delta^{18}O$ oscillations recognized in ODP-160-963A have just been misaligned by one D/O cycle length.

Although the chronostratigraphic database providing absolute age control on Pleistocene Mediterranean tephras is still relatively modest, there are at least two other tephras that bear on potential phase relationships among high-resolution paleoclimatic records in this interval. The first is the Campanian Ignimbrite from the Phlegrean Fields (Italy) dated at 39.28 ± 0.11 ka by $^{40}Ar/^{39}Ar$ (2σ internal error, calculated with FCT @ 27.8 Ma, De Vivo et al., 2001; recalculated to 39.93 ka with FCT @ 28.294 Ma). The Campanian Ignimbrite is correlated to Heinrich Event 4 (HE-4) in a number of high-resolution records in the Thyrrhenian and Adriatic Seas, the Monticchio varved lacustrine series (southern Italy), and the Lesvos and Tenaghi Philippon pollen records in Greece (e.g., Thunell et al., 1979; Ton-That et al., 2001; Watts et al., 2000; Muller et al., 2011; Margari et al., 2007). HE-4 correlates with the onset of Greenland Stadial 9 dated at ca. 40 ka in the GICC05 timescale, fully in line with the $^{40}Ar/^{39}Ar$ estimate. The second is the X-5 tephra layer that is correlated with a brief interstadial oscillation between the C24 and C23 cold events in the Monticchio pollen record that is itself correlated to Greenland Interstadial 24 (~ 108-106 ka). The ash was recently dated at Sulmona basin (Italy) by $^{40}Ar/^{39}Ar$ on sanidine at 106.2 ± 1.3 ka (2σ external), consistent with the varve age of the correlative tephra layer TM-25 (105.5 ± 1.1 ka) in the Monticchio sequence (Giaccio et al., 2012). Taken at face value, all these estimates appear closely concordant among the Greenland, Monticchio, and the $^{40}Ar/^{39}Ar$ records, suggesting that, within error of these timescales, there is no apparent phase lag among short-term climatic oscillations identified in the different archives. We emphasize, however, that is not yet obvious whether and to which extent potential errors such as discussed here ($^{40}Ar/^{36}Ar$ fractionation, $(^{40}Ar/^{39}Ar)_K$ correction factor, dead-time and mass-bias correction, etc.) were (or not) carefully evaluated and exhaustively propagated through these $^{40}Ar/^{39}Ar$ estimates to

ensure fully external errors as required to address phase relationships on a sub-millennial scale.

While the multi-proxy record of core ODP-160-963A potentially bears the resolution to address this issue, we also feel that more data from this (and other) high-resolution marine record(s) must be accumulated to firmly secure a shared climatic drive with possible near-millennial (or no) phase lag between the high-frequency Greenland variability and the Late Pleistocene Mediterranean deep-sea record. The near-millennial concordance established here between our $^{40}Ar/^{39}Ar$ estimate, the revised SPECMAP/LR04 tuning, and the Greenland template is in fact already strongly encouraging, especially considering the fitting assumptions involved and independent $^{40}Ar/^{39}Ar$ evidence from other Mediterranean tephras. Clearly, the new high-resolution $^{40}Ar/^{39}Ar$ age for GT and Y-6 provides a critical phase-fitting control point for such an endeavour and an improved long-range chronostratigraphic correlation tool throughout the Ionian Sea and the Eastern Mediterranean.

5. Conclusions

The handling of model age uncertainties and absolute time calibration is one of the more pressing and rapidly evolving subjects in paleoclimatology. Absolute temporal tie-points that are independent of tuning strategies or phasing assumptions are critical in this regard, particularly for recent marine records extending beyond the radiocarbon timescale. Together with emerging high-resolution U-Th chronologies from speleothems, corals, and tephras (Genty et al., 2010; Thompson and Goldstein, 2006; Vazquez and Lidzbarski, 2012), $^{40}Ar/^{39}Ar$ ages from large-scale volcanic events recorded onland and off-shore are bound to play an increasing role in upcoming phase-tuning strategies of Late Quaternary paleoclimate records.

The Green Tuff eruption is no exception to this rule and provides a geochemically unique and regionally extensive marker horizon across much of the central-eastern Mediterranean via its

putative Y-6 deep-sea equivalent. With an improved age estimate at 44.4 ± 0.6 ka (45.7 ± 1.0 ka, bias-corrected), the Green Tuff eruption ties Y-6 to O-isotope substage 3.13 at 44-45 ka in the high-resolution stack of Martinson et al. (1987) and Pisias et al. (1984), on par with termination of GI#12 in the Greenland record (Svensson et al., 2008). To the best of our knowledge, this is the first orbitally-independent radioisotopic tie-point reported for this marine substage in the Mediterranean.

Y-6 provides a timely pointer in an interval generally recorded as a muted δ^{18}O profile across the last glacial cycle and lacking high-resolution control both in marine and lacustrine records (e.g., Sulpizio et al., 2010). Our new ^{40}Ar/^{39}Ar tie-point uncovers a ± 3.1 ka root mean square deviation relative to the whole set of δ^{18}O-tied estimates considered in this study (Fig. 8). Such a figure reflects the error magnitude incurred in practice when tuning deep-sea δ^{18}O time-series just beyond the radiocarbon timescale. Our improved estimate represents the first reported ^{40}Ar/^{39}Ar age to be used with near-millennial resolution for checking phase relationships among marine, continental, and ice-core δ^{18}O records based on cores featuring Y-6 or in nearby marine records sharing correlative δ^{18}O time-series. The improved ^{40}Ar/^{39}Ar calibration of Y-6 via the Green Tuff argues for its formal integration into the INTIMATE tephra-framework (Blockley et al., 2012).

6. Acknowledgements

7. References

Aksu A.E., Jenner G., Hiscott R.N., İşler E.B. (2008) Occurrence, stratigraphy and geochemistry of Late Quaternary tephra layers in the Aegean Sea and the Marmara Sea. Mar. Geol. 252, 174–192.

Allen J.R.M. et al. (1999) Rapid environmental changes in southern Europe during the last glacial period. Nature 400, 740-743.

Anastasakis G., Pe-Piper G. (2006) An 18 m thick volcaniclastic interval in Pantelleria Trough, Sicily Channel, deposited from a large gravitative flow during the Green Tuff eruption. Mar. Geol. 231, 201–219.

Austin W.E.N., Hibbert F.D. (2012) Tracing time in the ocean: a brief review of chronological constraints (60-8 kyr) on North Atlantic marine event-based stratigraphies. Quat. Sci. Rev. 36, 28-37.

Bard E., Rostek F., Ménot-Combes G. (2004) Radiocarbon calibration beyond 20,000 ^{14}C yr B.P. by means of planktonic foraminifera of the Iberian margin. Quat. Res. 61, 204–214.

Blaauw M. (2012) Out of tune: the dangers of aligning proxy archives. Quat. Sci. Rev. 36, 38-49.

Blockley S.P.E., Lane C.S., Hardiman M., Rasmussen S.O., Seierstad I.K., Steffensen J.P., Svensson A., Lotter A.F., Turney C.S.M., Ramsey C.B., INTIMATE members (2012) Synchronisation of palaeoenvironmental records over the last 60,000 years, and an extended INTIMATE event stratigraphy to 48,000 b2k. Quat. Sci. Rev. 36, 2-10.

Cacho I., Grimalt J.O., Pelejero C., Canals M., Sierro F.J., Flores J.A., Shackleton N.J. (1999) Dansgaard–Oeschger and Heinrich event imprints in the Alboran Sea palaeotemperatures. Palaeoceanography 14, 698–705.

Calanchi N., Cattaneo A., Dinelli E., Gasparotto G., Lucchini F. (1998) Tephra layers in Late Quaternary sediments of the Central Adriatic Sea. Mar. Geol.,149, 191–209.

Caron B., Sulpizio R., Zanchetta G., Siani G., Santacroce R. (2010) The Late Holocene to Pleistocene tephrostratigraphic record of Lake Ohrid (Albania). C. R. Geosci., doi: 10.1016/j.crte.2010.03.007

Civetta L., Cornette Y., Gillot P.Y., Orsi G. (1988) The eruptive history of Pantelleria (Sicily Channel) in the last 50 ka. Bull. Volc. 50: 47-57.

Coble M.A., Grove M., Calvert A.T. (2011) Calibration of Nu-Instruments Noblesse multicollector mass spectrometers for argon isotopic measurements using a newly developed reference gas. Chem. Geol. 290, 75-87.

Combourieu Nebout N., Turon J.L., Zhan R., Capotondi L., Londeix L., Pahnke K. (2002) Enhanced aridity and atmospheric high-pressure stability over the western Mediterranean during the North Atlantic cold event of the past 50 ky. Geology 30, 863-866.

Cornette Y., Crisci G.M., Gillot P.Y., Orsi G. (1983) The recent volcanic history of Pantelleria: a new interpretation. In: Sheridan M.F. and Barberi F. (eds) Explosive volcanism. J. Volc. Geoth. Res. 17: 361-373.

De Vivo B., Rolandi G., Gans P.B., Calvert A., Bohrson W.A., Spera F.J., Belkin H.E. (2001) New constraints on the pyroclastic eruptive history of the Campanian volcanic Plain (Italy). Min. Pet. (2001) 73, 47-65.

Emeis K.-C, Robertson A.H.F., Richter C, and Shipboard Scientific Party (1996) ODP Site 963. Proc. Ocean Drilling Prog. Initial Reports 160, 55-84.

Emiliani C., Shackleton N.J. (1974) The Brunhes epoch: Isotopic paleotemperatures and geochronology. Science 183, 511-513.

Ferla P., Meli C. (2006) Evidence of Magma Mixing in the 'Daly Gap' of Alkaline Suites: a Case Study from the Enclaves of Pantelleria (Italy). J. Pet. 47, 1467-1507.

Fletcher W.J. et al. (2010) Millennial-scale variability during the last glacial in vegetation records from Europe. Quat. Sci. Rev. 29, 2839-2864.

Gansecki C.A., Mahood G.A., McWilliams M.O. (1996) $^{40}Ar/^{39}Ar$ geochronology of rhyolites erupted following collapse of the Yellowstone caldera, Yellowstone Plateau volcanic field: implications for crustal contamination. Earth Planet. Sci. Lett. 42: 91-107.

Genty D. et al. (2010) Isotopic characterization of rapid climatic events during OIS3 and OIS4 in Villars Cave stalagmites (SW-France) and correlation with Atlantic and Mediterranean pollen records. Quat. Sci. Rev. 29, 2799-2820.

Giaccio B., Nomade S., Wulf S., Isaia R., Sottili G., Cavuoto G., Galli P., Messina P., Sposato A., Sulpizio R., Zanchetta G. (2012) The late MIS 5 Mediterranean tephra markers: a reappraisal from peninsular Italy terrestrial records. Quat. Sci. Rev. 56, 31-45.

Hilgen F.J., Lourens L.J., Berger A., Loutre M.F. (1993) Evaluation of the astronomically calibrated time scale for the Late Pliocene and Earliest Pleistocene. Paleoceanography 8, 549-565.

Howell M. W., Thunell R. C., Di Stefano E., Sprovieri R., Tappa E. J., Sakamoto T. (1998) Stable isotope chronology and paleoceanographic history of Sites 963 and 964, Eastern Mediterranean sea. In: Emeis, K.-C., Robertson, A. H. F., Richter, C., Camerlenghi, A., Eds., Proceedings of the Ocean Drilling Pro- gram, Scientific Results 160, 167-180. College Station, TX: Ocean Drilling Program.

Huybers P., Wunsch C. (2004) A depth-derived Pleistocene age model: Uncertainty estimates, sedimentation variability, and nonlinear climate change. Paleoceanography 19, PA1028, doi:10.1029/2002PA000857

Incarbona A., Di Stefano E., Bonomo S. (2009) Calcareous nannofossil biostratigraphy of the central Mediterranean Basin during the last 430,000 years. Stratigraphy 6, 33-44.

Karner D.B, Levine J., Medeiros B.P., Muller R.A. (2002) Constructing a stacked benthic $\delta^{18}O$ record. Paleoceanography 17, doi:10.1029/2001PA000667.

Keller J., Ryan W.B.F., Ninkovich D., Altherr R. (1978) Explosive volcanic activity in the Mediterranean over the past 200000 years as recorded in deep-sea sediments. Geol. Soc. Am. Bull. 89, 591–604.

Kraml M. (1997) Laser-^{40}Ar/^{39}Ar-Datierungen an distalen Marinen Tephren des jung-quartären mediterranen Vulkanismus (Ionisches Meer, METEOR-Fahrt 25/4), Thesis, University of Freiburg, 216 pp.

Kuiper K.F., Deino A., Hilgen F. J., Krijgsman W., Renne P.R., Wijbrans J.R. (2008) Synchronizing Rock Clocks of Earth History. Science 320, 500-504.

Lisiecki L.E., Raymo M.E. (2005) A Pliocene-Pleistocene stack of 57 globally distributed benthic δ^{18}O records. Paleoceanography 20, PA1003, doi:10.1029/2004PA001071.

Lo Bello. Ph., Féraud G., Hall C.M., York D., Lavina P. (1987) ^{40}Ar/^{39}Ar step-heating and laser fusion dating of a Quaternary pumice from Neschers, Massif Central, France: The defeat of xenocrystic contamination. Chem. Geol. (Iso. Geosci. Sec.) 40, 39-53.

Lourens L.J. (2004) Revised tuning of Ocean Drilling Program Site 964 and KC01B (Mediterranean) and implications for the δ^{18}O, tephra, calcareous nannofossil, and geomagnetic reversal chronologies of the past 1.1 Myr. Paleoceanography 19, doi:10.1029/2003PA000997.

Lowe J.J., , Blockley S., Trincardi F., Asioli A., Cattaneo A., Matthews I.P., Pollard M., Wulf S. (2007) Age modelling of late Quaternary marine sequences in the Adriatic: Towards improved precision and accuracy using volcanic event stratigraphy. Continent. Shelf Res. 27, 560–582.

Mahood G.A., Hildreth W. (1986) Geology of the peralkaline volcano at Pantelleria, Strait of Sicily. Bull. Volc. 48: 143-172.

Margari V., Pyle D.M., Bryant C., Gibbard P.L. (2007) Mediterranean tephra stratigraphy revisited: results from a long terrestrial sequence on Lesvos Island, Greece. J. Volc. Geoth. Res. 163. 34–54.

Martinson D.G., Pisias N.G., Hays J.D., Imbrie J., Moore T.C., Shackleton N.J. (1987) Age dating and the orbital theory of the ice ages: Development of a high-resolution 0 to 300 000 year chronostratigraphy. Quat. Res. 27, 1–29.

Marvin R.F., Mehnert H.H., Noble D.C. (1970) Use of ^{36}Ar to evaluate the incorporation of air by ash flows. Geol. Soc. Am. Bull. 81, 3385-3392.

McDowell F. (1983) K-Ar dating: Incomplete extraction of radiogenic argon from alkali feldspar. Chem. Geol. 41,119–126.

Morgan L.E., Renne P.R., Taylor R.E., WoldeGabriel G. (2009) Archaeological age constraints from extrusion ages of obsidian: Examples from the Middle Awash, Ethiopia. Quat. Geochro. 4, 193–203.

Müller U.C., Prossa J., Tzedakis P.C., Gamble C., Kotthoff U., Schmiedl G., Wulff S., Christanis K. (2011) The role of climate in the spread of modern humans into Europe. Quat. Sci. Rev. 30, 273–279.

Narcisi B., Vezzoli L. (1999) Quaternary stratigraphy of distal tephra layers in the Mediterranean – an overview. Global Planet. Change 21, 31–50.

Negri A., Capotondi L., Keller J. (1999) Calcareous nannofossils, planktonic foraminifera and oxygen isotopes in the late Quaternary sapropels of the Ionian Sea. Mar. Geol. 157, 89–103.

Orsi G., Sheridan M.F. (1984) The Green Tuff of Pantelleria: rheoignimbrite or rheomorphic fall? Bull. Volcanol. 47, 611–626.

Paterne M., Guichard F., Duplessy J.C., Siani G., Sulpizio R., Labeyrie J. (2008) A 90,000–200,000 yrs marine tephra record of Italian volcanic activity in the Central Mediterranean Sea. J. Volc. Geoth. Res. 177, 187–196.

Paterne M., Guichard F., Labeyrie J. (1988) Explosive activity of the South Italian volcanoes durig the past 80000 years as determined by marine tephrochronology. J. Volc. Geoth. Res. 34, 153–172.

Paterne M., Guichard F., Labeyrie J., Gillot P.Y., Duplessy J.C. (1986) Tyrrhenian Sea tephrochronology of the oxigen isotope record for the past 60.000 years. Mar. Geol. 72, 259-285.

Pisias N.G., Martinson D.G., Moore T.C., Shackleton N.J., Prell W., Hays J.D., Boden G. (1984) High resolution stratigraphic correlation of benthic oxygen isotopic records spanning the last 300,000 years. Mar. Geol., 56, 119–136.

Piva A. et al. (2008) Climatic cycles as expressed in sediments of the PROMESS1 borehole PRAD1-2, central Adriatic, for the last 370 ka: 1. Integrated stratigraphy. Geochem. Geophys. Geosyst., doi:10.1029/2007GC001713.

Renne P.R., Mundil R., Balco G., Min K., Ludwig K.R. (2010) Joint determination of ^{40}K decay constants and ^{40}Ar*/^{40}K for the Fish Canyon sanidine standard, and improved accuracy for ^{40}Ar/^{39}Ar geochronology. Geochim. Cosmochim. Acta 74, 5349–5367.

Renne P.R., Balco G., Ludwig K.R., Mundil R., Min K. (2011) Response to the comment by W.H. Schwarz et al. on "Joint determination of ^{40}K decay constants and ^{40}Ar*/^{40}K for the Fish Canyon sanidine standard, and improved accuracy for ^{40}Ar/^{39}Ar geochronology" by P.R. Renne et al. (2010). Geochim. Cosmochim. Acta 75, 5097–5100.

Renne P.R., Swisher C.C., Deino A.L., Karner D.B., Owens T.L., DePaolo D.J. (1998) Intercalibration of standards, absolute ages and uncertainties in ^{40}Ar/^{39}Ar dating. Chem. Geol. 145, 117-152.

Rivera T.A., Storey M., Zeeden Ch., Hilgen F.J., Kuiper K. (2011) A refined astronomically calibrated ^{40}Ar/^{39}Ar age for Fish Canyon sanidine. Earth Planet. Sci. Lett. 311, 420–426.

Rotolo S.G., Scaillet S., La Felice S., Vita-Scaillet G. (2013) A revision of the structure and stratigraphy of pre-Green Tuff ignimbrites at Pantelleria (Strait of Sicily). J. Volc. Geoth. Res. 250, 61–74.

Scaillet S., Rotolo S.G., La Felice S., Vita-Scaillet G. (2011) High-resolution ^{40}Ar/^{39}Ar chronostratigraphy of the post-caldera (<20 ka) volcanic activity at Pantelleria, Sicily Strait. Earth Planet. Sci. Lett. 309, 280–290.

Scaillet S., Vita-Scaillet G. (2008) Oldest human footprints dated by Ar/Ar. Earth Planet. Sci. Lett. 275, 320-325.

Schmiedl G., Hemleben C., Keller J., Segl M. (1998) Impact of climatic changes on the benthic foraminiferal fauna in the Ionian Sea during the last 330,000 years. Paleoceanography 13, 447-458.

Shackleton N.J., Fairbanks R.G., Chiu T.-c., Parrenin F. (2004) Absolute calibration of the Greenland time scale: implications for Antarctic time scales and for δ^{14}C. Quat. Sci. Rev. 23, 1513–1522.

Siani G., Paterne M., Michel E., Sulpizio R., Sbrana A., Arnold M., Haddad G. (2001) Mediterranean Sea surface radiocarbon reservoir age Changes since the last glacial maximum. Science 294, 1917–1920.

Siani G., Sulpizio R., Paterne M., Sbrana A. (2004) Tephrostratigraphy study for the last 18,000 ^{14}C years in a deep-sea sediment sequence for the South Adriatic. Quat. Sci. Rev. 23, 2485–2500.

Sierro F.J., Hodell D.A., Curtis J.H., Flores J.A., Reguera I., Colmenero-Hidalgo E., Barcena M.A., Grimalt J.O., Cacho I., Frigola J., Canals M. (2005) Impact of iceberg melting on Mediterranean thermohaline circulation during Heinrich events. Paleoceanography 20, PA2019, doi:10.1029/2004PA001051.

Singer B.S., Guillou R., Jicha B.R., Laj C., Kissel C., Beard B.L., Johnson C.M. (2009) ^{40}Ar/^{39}Ar, K–Ar and ^{230}Th–^{238}U dating of the Laschamp excursion: A radioisotopic tie-point for ice core and climate chronologies. Earth Planet. Sci. Lett. 286, 80-88.

Smith P.E., York D., Chen Y., Evensen N.M. (1996) Single crystal ^{40}Ar–^{39}Ar dating of a Late Quaternary paroxysm on Kos, Greece: concordance of terrestrial and marine ages. Geophy. Res. Lett. 23, 3047–3050.

Spell T.L., Smith E.I., Sanford A., Zanetti K.A. (2001) Systematics of xenocrystic contamination: preservation of discrete feldspar populations at McCullough Pass Caldera revealed by ^{40}Ar/^{39}Ar dating. Earth Planet. Sci. Lett. 190, 153–165.

Sprovieri M., Di Stefano E., Incarbona A., Salvagio Manta D., Pelosi N., Ribera d'Alcalà M., Sprovieri R. (2012) Centennial- to millennial-scale climate oscillations in the Central-Eastern Mediterranean Sea between 20,000 and 70,000 years ago: evidence from a high-resolution geochemical and micropaleontological record. Quat. Sci. Rev. 46, 126-135.

Sulpizio R., Zanchetta G., D'Orazio M., Vogel H., Wagner B. (2010) Tephrostratigraphy and tephrochronology of lakes Ohrid and Prespa, Balkans. Biogeosci. Discuss. 7, 3931–3967.

Svensson A., Andersen K.K., Bigler M., Clausen H.B., Dahl-Jensen D., Davies S.M., Johnsen S.J., Muscheler R., Rasmussen S.O., Röthlisberger R., Steffensen J.P., Vinther B.M.: (2006) The Greenland Ice Core Chronology 2005, 15–42 ka. Part 2: comparison to other records. Quat. Sci. Rev. 25, 3258–3267.

Svensson A., Andersen K.K., Bigler M., Clausen H.B., Dahl-Jensen D., Davies S.M., Johnsen S.J., Muscheler R., Parrenin F., Rasmussen S.O., Rothlisberger R., Seierstad I., Steffensen J.P., Vinther B.M. (2008) A 60 000 year Greenland stratigraphic ice core chronology. Clim. Past 4, 47-57.

Tamburrino S. (2008) Mediterranean tephrochronology: new insights from high-resolution analyses of a 200.000 years long composite sedimentary record. PhD Thesis, Univ. Federico II, Napoli, 208 pp.

Tamburrino S., Insinga D.D., Sprovieri M., Petrosino P., Tiepolo M. (2012) Major and trace element characterization of tephra layers offshore Pantelleria Island: insights into the last 200 ka of volcanic activity and contribution to the Mediterranean tephrochronology. J. Quat. Sci. 27, 129–140.

Thompson W.G., Goldstein S.L. (2006) A radiometric calibration of the SPECMAP timescale. Quat. Sci. Rev. 25, 3207–3215.

Thunell R., Federman A., Sparks S., Williams D. (1979) The age, origin, and volcanological significance of the Y-5 ash layer in the Mediterranean. Quat. Res. 12, 241-253.

Ton-That T. (2001) ^{40}Ar/^{39}Ar dating of late Pleistocene marine and terrestrial tephra from the Tyrrhenian and Ionian Seas, Mediterranea: some implications for global climate changes. PhD Dissertation, Geneva Univ., 83 pp.

Ton-That T., Singer B., Paterne M. (2001) ^{40}Ar/^{39}Ar dating of latest Pleistocene (41 ka) marine tephra in the Mediterranean Sea: implications for global climate records. Earth Planet. Sci. Lett. 184, 645-658.

Turney C.S.M. et al. (2008) Geochemical characterization of Quaternary tephras from the Campanian Province, Italy. Quat. Int. 178, 288–305.

van Andel T.H. (2005) The ownership of time: approved ^{14}C calibration or freedom of choice? Antiquity 79, 944-948.

van den Bogaard P., Hall CM., Schminke H.-U., York D. (1987) [40]Ar/[39]Ar laser dating of single grains: ages of Quatemary tephra from the East Eifel volcanic field, FRG. Geophys. Res. Lett. 14, 1211-1214.

van den Bogaard P., Mocek B., Stavesand M. (1999) Chronology and composition of vocaniclastic ash layers in the central Tyrrhenian basin (Site 974). Proc. Ocean Drilling Prog., Scientific Results 161, 137-156.

Vazquez J.A., Lidzbarski M.I. (2012) High-resolution tephrochronology of the Wilson Creek Formation (Mono Lake, California) and Laschamp event using [238]U-[230]Th SIMS dating of accessory mineral rims. Earth Planet. Sci. Lett. 357–358, 54–67.

Vogel H., Zanchetta G., Sulpizio R., Wagner B., Nowaczyk N. (2010) A tephrostratigraphic record for the last glacial – interglacial cycle from Lake Ohrid, Albania and Macedonia. J. Quat. Sci. 25, 320–338.

von Dobeneck T., Schmieder F. (1999) Using rock magnetic proxy records for orbital and extended time-series analyses into the super- and sub-Milankovitch bands. In: Fischer G. & Wefer G. (eds.), Use of Proxies in Paleoceanography - Examples from the South Atlantic, Springer, Berlin, Heidelberg, pp. 601-633.

Waelbroeck C., Frank N., Jouzel J., Parrenin F., M.asson-Delmotte V., Genty D. (2008) Transferring radiometric dating of the last interglacial sea level high stand to marine and ice core records. Earth Planet. Sci. Lett. 265, 183–194.

Wallace P.J., Dufek J., Anderson A.T., Zhang Y. (2003) Cooling rates of Plinian-fall and pyroclastic-flow deposits in the Bishop Tuff: inferences from water speciation in quartz-hosted glass inclusions. Bull. Volc. 65, 105–123.

Watts W.A., Allen J.R.M., Huntley B. (2000) Palaeoecology of three interstadial events during oxygen-isotope Stages 3 and 4: a lacustrine record from Lago Grande di Monticchio, southern Italy. Palaeogeo., Palaeoclim., Palaeoeco. 155, 83–93

Westerhold T., Röhl U., Laskar J. (2012) Time scale controversy: Accurate orbital calibration of the early Paleogene. Geochem. Geophys. Geosyst. 13, Q06015, doi:10.1029/2012GC004096.

White J.C., Parker D.F., Ren M. (2009) The origin of trachyte and pantellerite from Pantelleria, Italy: Insights from major element, trace element, and thermodynamic modelling. J. Volc. Geoth. Res. 179, 33–55.

Williams R. (2010) Emplacement of radial pyroclastic density currents over irregular topography: the chemically-zoned, low aspect-ratio Green Tuff ignimbrite, Pantelleria, Italy. PhD Dissertation, Leicester Univ., 224 pp.

Wolff J.A., Wright J.V. (1981) Formation of the Green Tuff, Pantelleria. Bull. Volc. 44, 681–690.

Wulf S., Kraml M., Brauer A., Keller J., Negendank J.F.W. (2004) Tephrochronology of the 100 ky lacustrine sediment record of Lago Grande di Monticchio (Southern Italy). Quat. Int. 122, 7–30.

Wulf S., Kraml M., Brauer A., Keller J. (2008) Towards a detailed distal tephrostratigraphy in the Central Mediterranean: The last 20,000 yrs record of Lago Grande di Monticchio. J. Volc. Geoth. Res. 177, 118–132.

Wunsch C. (2006) Abrupt climate change: An alternative view. Quat. Res. 65, 191-203.

Zanchetta G., Sulpizio R., Giaccio B., Siani G., Paterne M., Wulf S., D'Orazio M. (2008) The Y-3 Tephra: a Last Glacial stratigraphic marker for the Central Mediterranean Basin. J. Volc. Geoth. Res. 177, 145–154.

Figure and Table captions

Fig. 1. Simplified geological map of Pantelleria (adapted from Mahood and Hildreth, 1986) with inset showing general dispersal pattern of Y-6 tephra bed in the central-eastern Mediterranean (from Margari et al., 2007). Location of sampling site at Cala Cinque Denti indicated by star. Location of deep-sea and lacustrine cores reporting distal occurrences indicated in the inset. *(To reproduce in color in the online webversion only.)*

Fig. 2. Spectacular exposure of the Green Tuff mantling older units over the Salto La Vecchia caldera scarp (ca. 140 ka, Rotolo et al., 2013), south of Pantelleria. Note characteristic pistachio-green color of lower Member C and progressive rheomophic thickening of the compound ignimbrite flow downslope of the scarp (particularly well expressed in the upper brownish Member D). Lower left picture: close-up of the contact with people making for scale. Lower right picture: member zonation of the Green Tuff at sample location PAN 0674 near Cala Cinque Denti (arrow: dark-green basal vitrophyre lining Member C; hammer length is about 30 cm). *(To reproduce in color in the online webversion only.)*

Fig. 3. Whole rock and glass-shard major element oxide composition of the Green tuff (GT) and its distal deep-sea tephra correlative (Y-6). Numbering of data sources on ordinal scale: [1-5] this study (1 = basal pumice fall, 5 = trachytic phenocryst-rich top), [6] Keller et al. (1978), [7] Anastasakis and Pe-Piper (2006), [8-9] Vogel et al. (2010), [10-11] Margari et al. (2007), [12-13] Tamburrino (2008), [14] Civetta et al. (1988), [15] Ferla and Meli (2006), [16-17] White et al. (2009). *(To reproduce in color in the online webversion only.)*

Fig. 4. Trace element pattern of glass composition of the proximal Green Tuff (GT) deposit and its distal outboard tephra equivalents (Y-6 and correlative). Width of the pattern for the peralkaline-rhyolite component (PANT) reflects the range in composition published in the

literature. TRACH is the trachyte component of the zoned tephra. Data sources as in Fig. 3. *(To reproduce in color in the online webversion only.)*

Fig. 5. Probability density and Gauss-plot of pooled ^{40}Ar/^{39}Ar ages of the Green Tuff. Error bars of individual ages are 1σ. Pooled age in density plot is the weighted mean age (2σ) as reported in Table 1. Age estimate (2σ) in Gauss-plot is derived from best fit parameters of straight-line fit through the data array. Large-error ^{40}Ar/^{39}Ar ages in upper tail of the distribution are derived from low-T degassing steps (i.e., with higher atmospheric contamination). *(To reproduce in color in the online webversion only.)*

Fig. 6. Inverse isochron plots of pooled ^{40}Ar/^{39}Ar data. *(To reproduce in color in the online webversion only.)*

Fig. 7. Orbitally-tied δ^{18}O age models of selected Mediterranean deep-sea cores featuring the Y-6 tephra layer. Kinked horizontal red line: age-depth position of Y-6 through the respective cores with blow up (right) showing the high-resolution δ^{18}O record of core ODP-160-963A tied to the NGRIP (GICC05) template by Tamburrino (2008). Superimposed green curves for core ODP-160-963A represent original data (light green) along with a 5-point moving average (bold green) of the composite δ^{18}O record from Howell et al. (1998) tied to LR04 (high-resolution δ^{18}O-benthic stack of Liesecki and Raymo, 2005). *(To reproduce in color in the online webversion only.)*

Fig. 8. Summary of K-Ar and ^{40}Ar/^{39}Ar data for the Green Tuff and δ^{18}O-tuned and biozone/radiocarbon bracketing of tephra Y-6 age. Key to numbering of reported data: [1, 2, 3]: K-Ar (Cornette et al., 1983); [4, 5]: K-Ar (Mahood and Hildreth, 1986); [6]: pooled isochron ^{40}Ar/^{39}Ar age of Ton-That (2001) recalculated (this study); [7]: Core RC9-191 (Keller et al., 1978; tuned to δ^{18}O age model of Emiliani and Shackleton, 1974 = ES74); [8]: Core M25/4-13 (Kraml, 1997; tuned to δ^{18}O stack of Martinson et al., 1987 = SPECMAP);

[9]: Core M25/4-12 (Kraml, 1997; SPECMAP tuning); [10]: Lesvos tephra sequence, Greece (Margari et al., 2007; biozone/radiocarbon bracketing = Bio+14C); [11]: GT volcaniclastic sequence, Pantelleria Trough (Bio+14C, Anastasakis and Pe-Piper, 2006); [12]: Core M25/4-12 (SPECMAP tuning; revised by Anastasakis and Pe-Piper, 2006); [13]: Core ODP 160-963A off SW Sicily (NGRIP-GICC05 tuning, Tamburrino, 2008); [14]: Core ODP 160-963A off SW Sicilia (SPECMAP tuning; Tamburrino et al., 2012); [15]: Core M25/4-13 (revised SPECMAP tuning, this study); [16]: Core M25/4-12 (revised SPECMAP tuning, this study); [17]: Core ODP 160-963A (composite $\delta^{18}O$ record tuned to LR04, this study). Vertical red line: revised $^{40}Ar/^{39}Ar$ age estimate of 45.7 ka (this study) with 2σ error band. *(To reproduce in color in the online webversion only.)*

Table 1. Summary of $^{40}Ar/^{39}Ar$ age determinations of the Green Tuff.

Table 2. Geochemical composition of the Green Tuff. Whole rock (glass) XRF analyses of the Green Tuff sequence. Peralkalinity Index = Na$_2$O+K$_2$O)/Al$_2$O$_3$ molar. L.O.I. = loss on ignition. n.a. = not analyzed.

Table 3. Summary of mineral chemistry determined by SEM-EDS (phenocrysts only) of the Green Tuff sequence. Peralkalinity Index = Na$_2$O+K$_2$O)/Al$_2$O$_3$ molar. aenig = aenigmatite; qz = quartz; mag = magnetite; ilm = ilmenite.

Table 4. Member subdivision and facies description of the Green Tuff sequence. * Thickness at Cala Cinque Denti.

Table 5. Published and revised (this study) radiochronologic and astronomical age estimates for the Green Tuff, Pantelleria, and its distal tephra correlative Y-6. ES74: Emiliani and Shackleton (1974). LR04: $\delta^{18}O$ stack of Liesecki and Ramo (2005). SPECMAP: $\delta^{18}O$ stack of Martinson et al. (1987). Bio+14C: biozone and radiocarbon bracketing. NGRIP: GICC05

timescale of Svensson et al. (2006). * Pooled Ar/Ar isochron age recalculated from Ton-That

(2001) using revised decay constant and monitor values of Renne et al. (2010, 2011)

Supplemental file S1. ^{40}Ar/^{39}Ar analytical procedures and results

Anorthoclase crystals were extracted by crushing, sieving, magnetic and heavy-liquid seperation, and handpicking under a binocular microcope. They were cleaned by ultrasonic etching in a dilute (2-5 %) hydrofluoridric solution for 3-5 min, followed by ultrasonic rinse in acetone, ethanol, and deionized water. Final concentrates were refined in the 1.0-1.6 mm size fraction by handpicking under a binocular microcope to screen out inclusion-rich or melt-coated specimens. All analyzed grains are pristine with well preserved crystal faces and/or very sharp broken surfaces.

About 150 mg of each sample separate were individually loaded in three 4 mm I.D. holes machined into a 11 mm O.D., 3 mm thick, Al-irradiation disks. Samples were co-irradiated with the irradiation monitors ACR-2 and TCR loaded in smaller adjacent pits bracketing the three sample locations. The disks, each loaded with one sample, were individually wrapped in domestic Al-foil, then stacked on top of each other in an irradiation vessel fitting into a Cd-lined irradiation can provided by the reactor facility for irradiation in the fast-neutron port β_1 of the Osiris nuclear reactor (CEA, Saclay). The disks were stacked with their respective monitor locations aligned along the axis of the can pile to provide accurate X-Y-Z control on the flux gradient. Corrections for isotopic interferences from K, Ca, and Cl were applied using production ratios listed in Scaillet et al. (2008, 2011) and this study. Correction for the flux gradient is done by fitting the *J*-factor along the can axis for each of the three monitor positions aligned coaxial with the can length, and by interpolation between best-fit *J*-values bracketing the sample position at each level. Apparent ^{40}Ar/^{39}Ar ages tabulated and plotted for each aliquot account for vertical and lateral flux gradients (and intra-sample ^{39}Ar$_K$-yield variations) by normalization to a common *J*.

After baking overnight at 180 °C, small clusters weighing ca. 2-8 mg (comprising about 10 to 50 crystals, depending on grain size) were individually analyzed with a continuous 20 W Synrad® CO_2 laser source coupled to a noble gas MM5400 mass-spectrometer operated in pulse-counting mode (Scaillet et al., 2008, 2011). A two-step degassing procedure was applied. (i) A first low-T step to remove essentially all surface-bound (non-radiogenic) component trapped in defects or surface-adhering residual glass, and/or in fluid inclusions decrepitating at low temperature (< 600-700 °C). (ii) A higher-T fusion step until complete melting of the mineral aggregate into small coalescing melt beads (> 1450-1500 °C). Using greater sample sizes to extract more steps was not considered practical for reasons outlined in Scaillet et al. (2011). Released gases were purified prior to gas admission into the mass-spectrometer by exposure for 10 min on two air-cooled GP50 S.A.E.S.® getter cartridges featuring a Zr-Al St101® alloy held at 250 °C.

Age were calculated using in-house software (Scaillet, 2000) based on conventional isotope abundances (Steiger and Jäger, 1977) and monitor and decay constants updated by Renne et al. (2010, 2011). Raw data were regressed to apparent ages using

the atmospheric ratios of $^{40}Ar/^{36}Ar$ = 295.5 (cf. McDougall and Harrison, 1999). Application of the recently revised value of 298.56 ± 0.1 (Lee et al., 2006) is irrelevant for this study as discussed in Scaillet et al. (2011). Monitoring of the instrumental mass-fractionation is achieved by daily calibration of the atmospheric $^{40}Ar/^{36}Ar$ isotope ratio on air shots interspersed with the unknowns at different peak intensities to correct for nonlinearity and counting dead-time (for every isotope) using in-house software (Scaillet et al., 2008, 2011). The mass discrimination factor varied between 0.9984 ± 0.0016 (2σ) and 0.9967 ± 0.0016 (2σ) pmu, assuming a linear mass-bias law. Unless otherwise stated, age errors are plotted and tabulated at 2σ and include corrections for (1) counting dead-time for every isotope, (2) system blanks, (3) mass-discrimination, (4) post-irradiation decay of ^{39}Ar, ^{37}Ar, and ^{36}Cl, (5) isotope interference corrections from K, Ca and Cl, (6) atmospheric contamination, (7) neutron-flux gradients, and (8) monitor's age error.

Additional references not cited in main text

Lee J.-Y., Marti K., Severinghaus J.P., Kawamura K., Yoo H.-S., Lee J.B., Kim J.S. (2006) A redetermination of the isotopic abundances of atmospheric Ar. Geochim. Cosmochim. Acta 70: 4507-4512.

McDougall I., Harrison T.M. (1999) Geochronology and thermochrology by the $^{40}Ar/^{39}Ar$ method, 2nd edition. Oxford University Press, Oxford.

Scaillet S. (2000) Numerical error analysis in $^{40}Ar/^{39}Ar$ dating. Chem. Geol. 162: 269-298.

Steiger R.H., Jäger E. (1977) Subcommission on geochronology: convention on the use of decay constants in geo- and cosmochronology. Earth Planet. Sci. Lett. 6, 359–362.
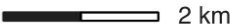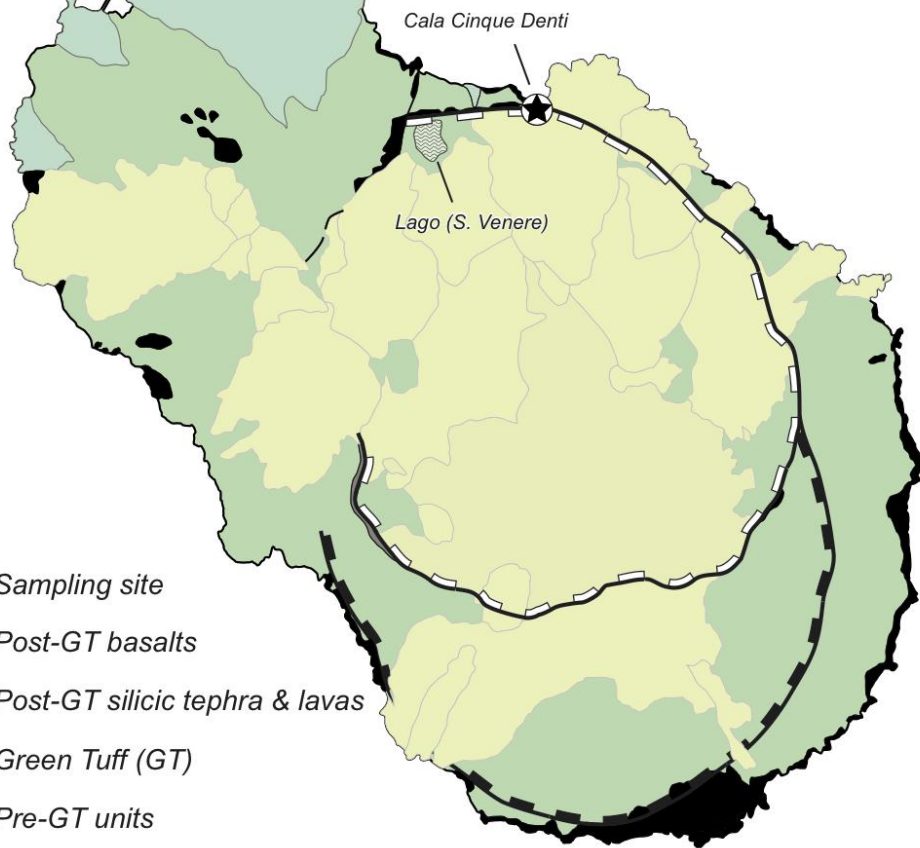
Supplemental Table S1. Analytical Ar/Ar data

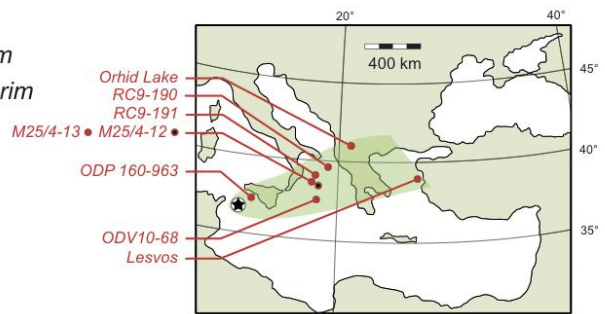**Table S1**. Ar/Ar results

Run #	$^{39}Ar_K$ (V)	$^{36}Ar_{atm}/^{39}Ar_K$ (± 1σ)			$^{37}Ar_{Ca}/^{39}Ar_K$ (± 1σ)			%$^{40}Ar^*$	$^{40}Ar^*/^{39}Ar_K$ (± 1σ)			Age (ka) (± 1σ)		
								PAN 06-057 (mean J = 1.375E-04)						
# 1	0.0052	0.00168	±	0.00002	0.0027	±	0.0004	26.6	0.180	±	0.012	45.00	±	2.88
# 2	0.0048	0.00173	±	0.00002	0.0020	±	0.0005	26.1	0.180	±	0.008	45.15	±	2.00
# 3	0.0052	0.00158	±	0.00003	0.0014	±	0.0007	27.5	0.177	±	0.010	44.29	±	2.54
# 4	0.0049	0.00156	±	0.00003	0.0010	±	0.0007	28.4	0.183	±	0.010	45.73	±	2.49
# 5	0.0047	0.01286	±	0.00006	0.0013	±	0.0007	4.7	0.187	±	0.024	46.77	±	5.98
# 6	0.0055	0.00167	±	0.00002	0.0013	±	0.0006	24.9	0.163	±	0.008	39.89	±	1.91
# 7	0.0043	0.00215	±	0.00003	0.0020	±	0.0006	20.1	0.160	±	0.011	40.02	±	2.87
# 8	0.0046	0.00390	±	0.00003	0.0033	±	0.0006	13.2	0.176	±	0.014	42.98	±	3.30
# 9	0.0050	0.00311	±	0.00003	0.0017	±	0.0006	14.5	0.155	±	0.013	38.87	±	3.27
# 10	0.0054	0.00200	±	0.00002	0.0019	±	0.0005	22.1	0.168	±	0.017	41.02	±	4.21
# 11	0.0053	0.00773	±	0.00005	0.0022	±	0.0008	7.1	0.175	±	0.019	42.73	±	4.65
# 12	0.0079	0.00161	±	0.00002	0.0000	±	0.0000	26.0	0.168	±	0.006	41.99	±	1.38
# 13	0.0067	0.00131	±	0.00002	0.0000	±	0.0000	30.6	0.170	±	0.005	42.55	±	1.37
# 14	0.0053	0.00195	±	0.00002	0.0000	±	0.0000	23.4	0.176	±	0.007	44.06	±	1.71
Total	0.0748	0.00306	±	0.00001	0.0014	±	0.0001	16.0	0.172	±	0.003	43.14	±	0.82
								PAN 06-074 (mean J = 1.421E-04)						
# 1	0.0010	0.00110	±	0.00008	0.0035	±	0.0027	31.2	0.147	±	0.030	38.27	±	7.73
# 2	0.0062	0.00070	±	0.00002	0.0005	±	0.0005	46.4	0.178	±	0.008	46.50	±	2.07
# 3*	0.0009	0.00195	±	0.00016	0.0042	±	0.0034	29.9	0.246	±	0.069	64.27	±	18.06
# 4	0.0063	0.00083	±	0.00002	0.0003	±	0.0005	43.2	0.187	±	0.010	48.79	±	2.65
# 5*	0.0009	0.00224	±	0.00015	0.0034	±	0.0033	28.5	0.263	±	0.066	68.63	±	17.22
# 6	0.0048	0.00112	±	0.00002	0.0002	±	0.0005	36.8	0.191	±	0.010	49.99	±	2.70
# 7*	0.0009	0.00255	±	0.00014	0.0019	±	0.0024	22.8	0.223	±	0.055	58.19	±	14.40
# 8	0.0053	0.00093	±	0.00002	0.0007	±	0.0004	39.8	0.181	±	0.008	47.27	±	2.02
# 9*	0.0005	0.00252	±	0.00015	0.0067	±	0.0043	24.4	0.241	±	0.062	62.82	±	16.31
# 10	0.0075	0.00218	±	0.00002	0.0004	±	0.0003	20.7	0.169	±	0.007	44.05	±	1.75
# 11*	0.0005	0.00249	±	0.00019	-0.0004	±	0.0076	22.8	0.217	±	0.068	53.35	±	16.78
# 12	0.0086	0.00952	±	0.00004	0.0002	±	0.0004	6.6	0.198	±	0.054	48.59	±	13.25
# 13*	0.0004	0.00270	±	0.00025	0.0217	±	0.0046	23.8	0.249	±	0.090	61.21	±	22.08
# 14	0.0077	0.00063	±	0.00001	0.0005	±	0.0002	50.1	0.187	±	0.006	45.86	±	1.42
# 15*	0.0004	0.00574	±	0.00034	0.0041	±	0.0065	11.6	0.223	±	0.121	54.79	±	29.79
# 16	0.0067	0.00165	±	0.00002	0.0002	±	0.0004	27.2	0.182	±	0.009	44.74	±	2.18
# 17*	0.0003	0.00207	±	0.00042	0.0032	±	0.0082	20.7	0.160	±	0.150	39.18	±	36.74
# 18	0.0066	0.00123	±	0.00002	0.0009	±	0.0002	34.4	0.191	±	0.007	46.94	±	1.70
# 19*	0.0004	0.00137	±	0.00020	0.0099	±	0.0050	38.3	0.252	±	0.072	65.79	±	18.72
# 20	0.0053	0.00105	±	0.00002	0.0005	±	0.0004	37.5	0.186	±	0.007	48.44	±	1.72
# 21	0.0052	0.00167	±	0.00003	0.0009	±	0.0008	27.9	0.191	±	0.011	47.02	±	2.67
# 22	0.0033	0.00121	±	0.00006	0.0019	±	0.0008	33.8	0.183	±	0.022	46.52	±	5.67
# 23	0.0066	0.00197	±	0.00002	0.0011	±	0.0004	22.5	0.169	±	0.007	44.70	±	1.82
# 24	0.0052	0.00954	±	0.00005	0.0007	±	0.0004	4.5	0.134	±	0.017	35.55	±	4.54
# 25	0.0045	0.00501	±	0.00003	0.0000	±	0.0009	9.6	0.157	±	0.010	41.66	±	2.74
# 26	0.0048	0.00429	±	0.00003	0.0017	±	0.0006	10.8	0.153	±	0.012	40.45	±	3.10
# 27	0.0036	0.00067	±	0.00004	0.0019	±	0.0008	39.7	0.130	±	0.016	34.42	±	4.26
# 28	0.0053	0.00143	±	0.00003	0.0011	±	0.0006	25.5	0.145	±	0.011	38.28	±	3.03
# 29	0.0042	0.00163	±	0.00003	0.0000	±	0.0000	25.5	0.165	±	0.008	43.75	±	2.03
Total	0.1140	0.00261	±	0.00001	0.0006	±	0.0001	18.7	0.177	±	0.005	46.93	±	1.30
								PAN 06-074bis (mean J = 1.341E-05)						
# 1	0.0002	0.01518	±	0.00045	0.0021	±	0.0008	29.7	1.891	±	0.134	45.78	±	3.23
# 2	0.0002	0.03160	±	0.00044	0.0013	±	0.0008	16.1	1.795	±	0.131	43.45	±	3.17
# 3	0.0002	0.00911	±	0.00053	0.0005	±	0.0011	41.8	1.935	±	0.159	46.85	±	3.85
# 4	0.0002	0.01646	±	0.00056	0.0014	±	0.0011	28.5	1.940	±	0.167	46.96	±	4.05
# 5	0.0002	0.02291	±	0.00047	0.0012	±	0.0010	21.9	1.897	±	0.141	45.92	±	3.42
# 6	0.0003	0.02988	±	0.00037	0.0013	±	0.0006	16.3	1.714	±	0.109	41.49	±	2.65
# 7	0.0003	0.01136	±	0.00032	0.0007	±	0.0006	34.1	1.737	±	0.097	42.68	±	2.39
# 8	0.0003	0.01214	±	0.00036	0.0021	±	0.0006	33.6	1.814	±	0.109	44.55	±	2.68
# 9	0.0002	0.01299	±	0.00051	0.0015	±	0.0010	32.0	1.804	±	0.152	44.31	±	3.72
# 10	0.0003	0.00903	±	0.00039	0.0012	±	0.0007	40.2	1.790	±	0.118	43.98	±	2.89
# 11	0.0002	0.01272	±	0.00043	0.0005	±	0.0009	32.7	1.822	±	0.127	44.75	±	3.12
# 12	0.0002	0.01180	±	0.00035	0.0009	±	0.0008	35.2	1.893	±	0.105	46.51	±	2.58
# 13	0.0002	0.00760	±	0.00043	0.0020	±	0.0008	46.0	1.910	±	0.130	45.81	±	3.11
# 14	0.0002	0.00869	±	0.00052	0.0014	±	0.0009	41.5	1.819	±	0.155	43.63	±	3.72
# 15	0.0002	0.01323	±	0.00048	0.0019	±	0.0011	32.3	1.864	±	0.144	44.71	±	3.46
# 16	0.0004	0.01289	±	0.00023	0.0011	±	0.0005	33.0	1.875	±	0.068	44.97	±	1.64
# 17	0.0004	0.01383	±	0.00023	0.0017	±	0.0006	31.5	1.875	±	0.070	44.97	±	1.67
# 18	0.0004	0.01856	±	0.00028	0.0011	±	0.0005	25.5	1.879	±	0.085	45.41	±	2.06
# 19	0.0002	0.01040	±	0.00047	0.0013	±	0.0009	37.4	1.836	±	0.145	44.38	±	3.51
# 20	0.0002	0.01312	±	0.00041	0.0016	±	0.0007	32.9	1.899	±	0.126	45.90	±	3.05
# 21	0.0002	0.03312	±	0.00042	0.0012	±	0.0006	15.3	1.766	±	0.128	43.36	±	3.14
# 22	0.0002	0.01132	±	0.00045	0.0017	±	0.0009	35.8	1.864	±	0.139	45.78	±	3.40
# 23	0.0002	0.01020	±	0.00040	0.0013	±	0.0008	37.9	1.840	±	0.121	45.18	±	2.96
# 24	0.0003	0.02223	±	0.00042	0.0006	±	0.0007	19.9	1.634	±	0.126	40.12	±	3.11
# 25	0.0002	0.00785	±	0.00039	0.0011	±	0.0008	43.4	1.775	±	0.120	43.59	±	2.95
# 26	0.0002	0.00666	±	0.00038	0.0020	±	0.0008	48.9	1.884	±	0.116	45.11	±	2.79
# 27	0.0002	0.01591	±	0.00043	0.0012	±	0.0008	28.2	1.845	±	0.132	44.19	±	3.16
# 28	0.0001	0.00786	±	0.00057	0.0006	±	0.0014	48.1	2.156	±	0.172	51.63	±	4.11
# 29	0.0001	0.00826	±	0.00061	0.0023	±	0.0014	43.7	1.892	±	0.181	45.31	±	4.33
# 30	0.0001	0.01305	±	0.00067	0.0012	±	0.0016	31.9	1.803	±	0.198	43.18	±	4.75
Total	0.0068	0.01469	±	0.00008	0.0013	±	0.0001	29.8	1.842	±	0.023	44.10	±	1.94

Totals computed from summed volumes with linear error propagation; they may differ from integrated estimates derived from statistically pooling individual runs and quadratically averaging individual errors.

(*) Runs flagged with an asterisk are low-T pre-degassing steps measured prior to fusion; all other are fusion steps preceded by low-T degassing.

La Vecchia caldera rim

Cinque Denti caldera rim

2 km

Orhid Lake
RC9-190
RC9-191
M25/4-13 ● ● M25/4-12
ODP 160-963
ODV10-68
Lesvos

400 km

Cala Cinque Denti

Lago (S. Venere)

★ Sampling site

Post-GT basalts

Post-GT silicic tephra & lavas

Green Tuff (GT)

Pre-GT units

44.9 ± 0.6

44.4 ± 0.6

N = 73

GREEN TUFF
Pooled & unscreened
45.7 ± 1.0 ka (2σ)
$(^{40}\text{Ar}/^{36}\text{Ar})_{\text{trapped}} = 292.7 \pm 2.0$ (2σ)
MSWD = 0.90
N = 73

#	Method	
1	K-Ar	
2	K-Ar	
3	K-Ar	
4	K-Ar	
5	K-Ar	
6	Ar/Ar	
7	$\delta^{18}O$ vs. ES74	
8	$\delta^{18}O$ vs. SPECMAP	
9	$\delta^{18}O$ vs. SPECMAP	
10	Bio+14C	
11	Bio+14C	
12	$\delta^{18}O$ vs. SPECMAP	
13	$\delta^{18}O$ vs. NGRIP	
14	$\delta^{18}O$ vs. SPECMAP	
15	$\delta^{18}O$ vs. SPECMAP	
16	$\delta^{18}O$ vs. SPECMAP	
17	$\delta^{18}O$ vs. LR04	

← Ar/Ar ± 2σ (this study)
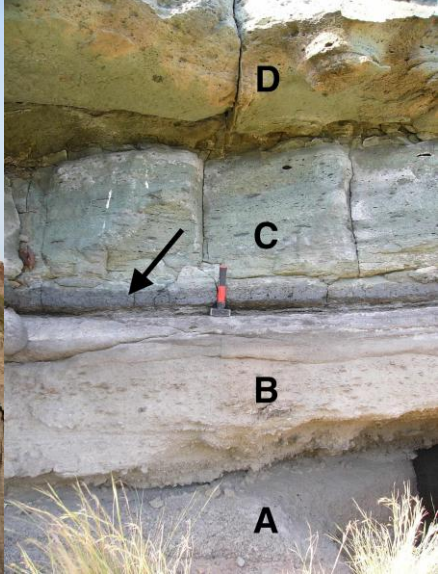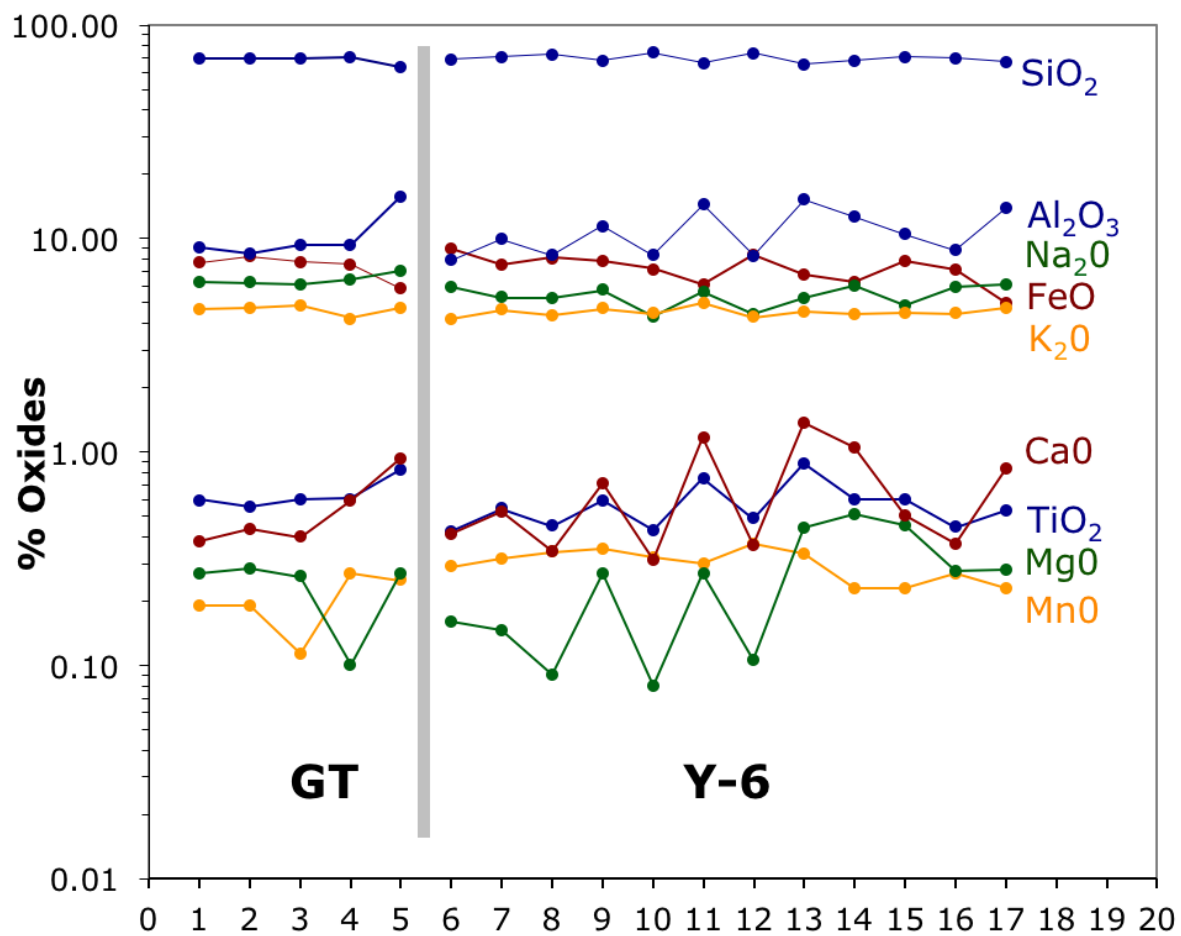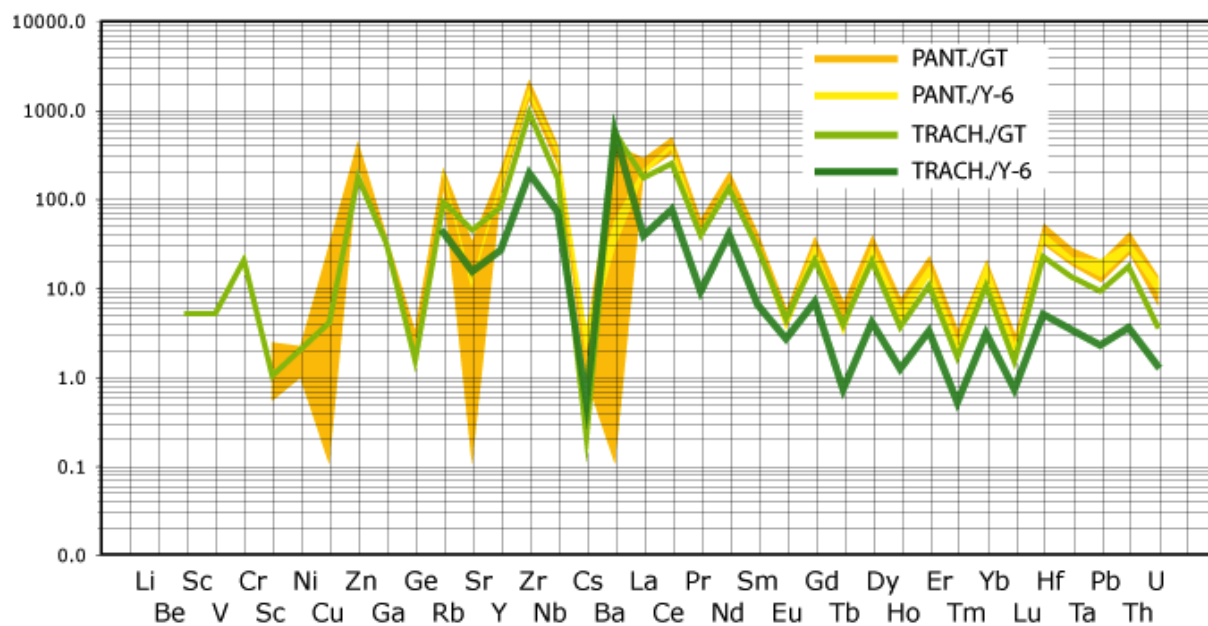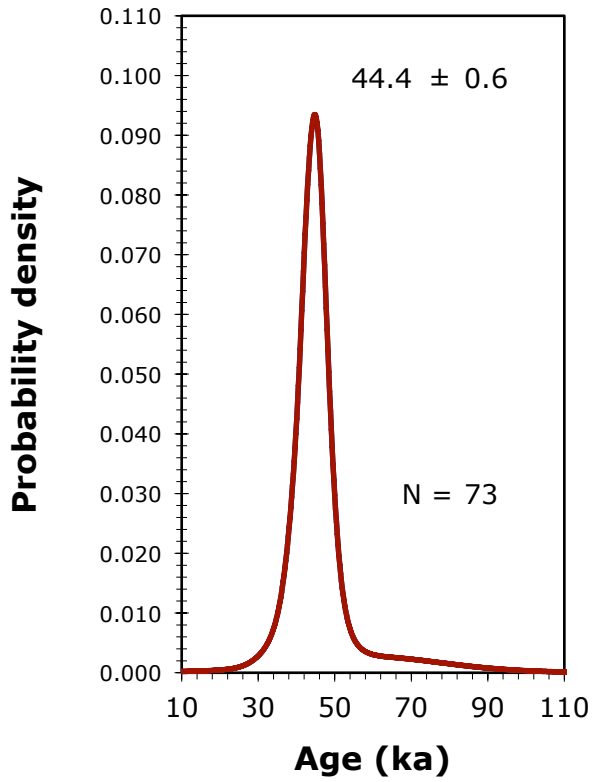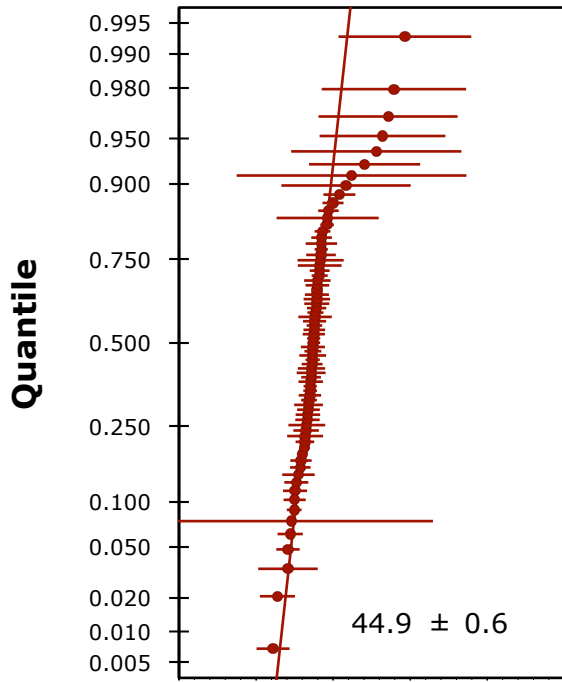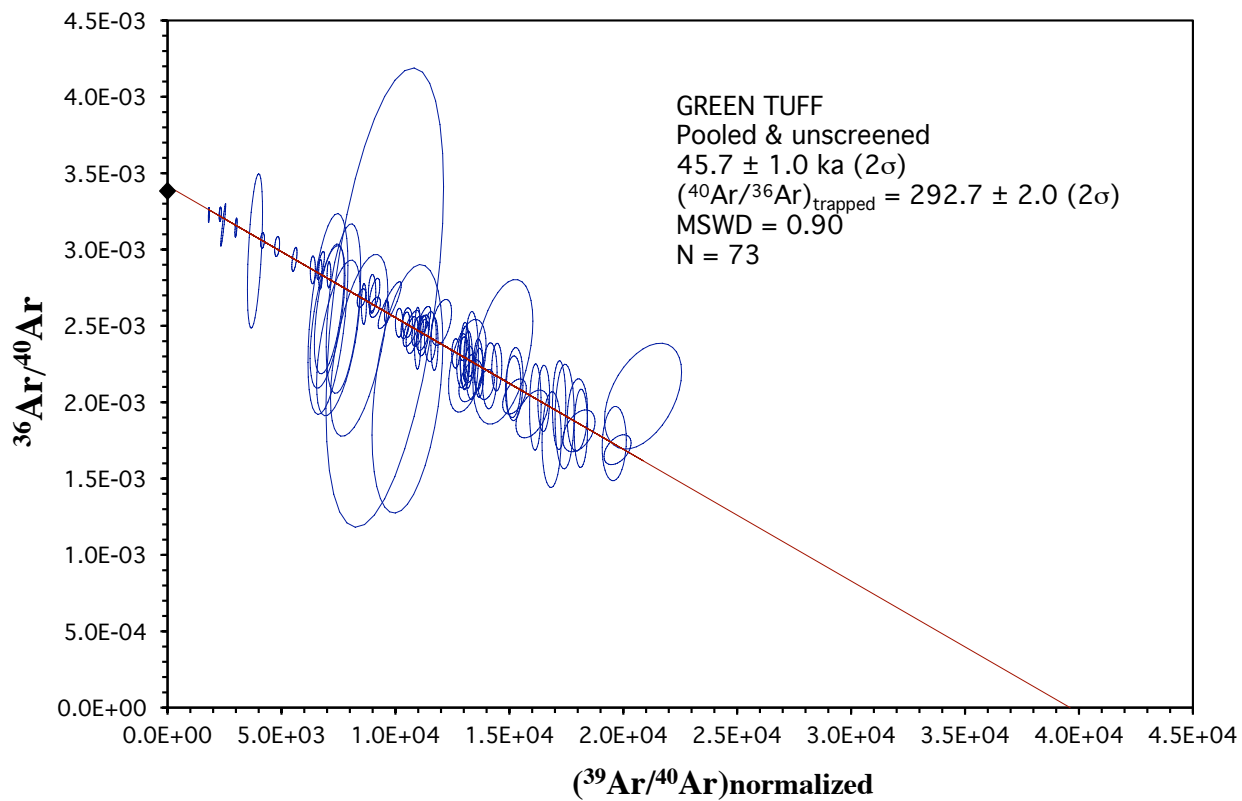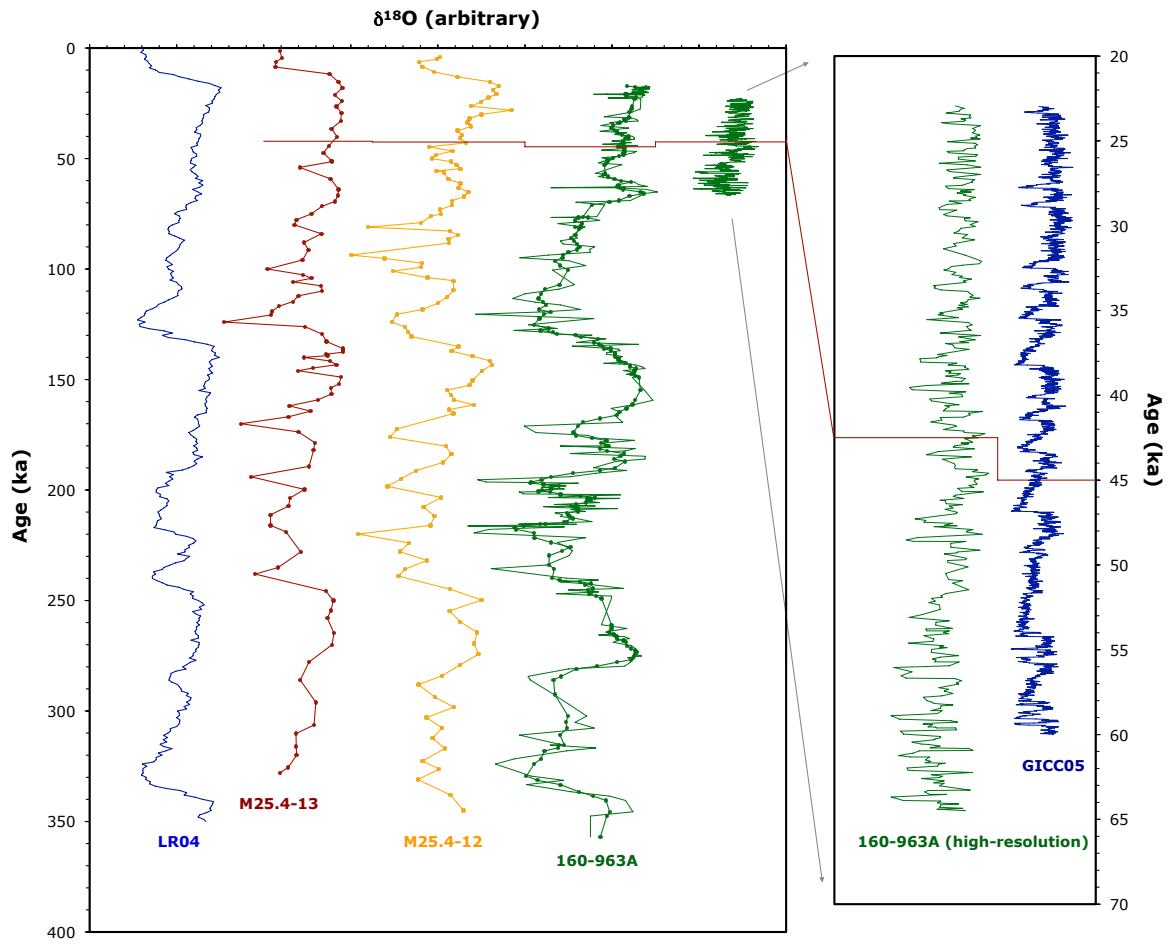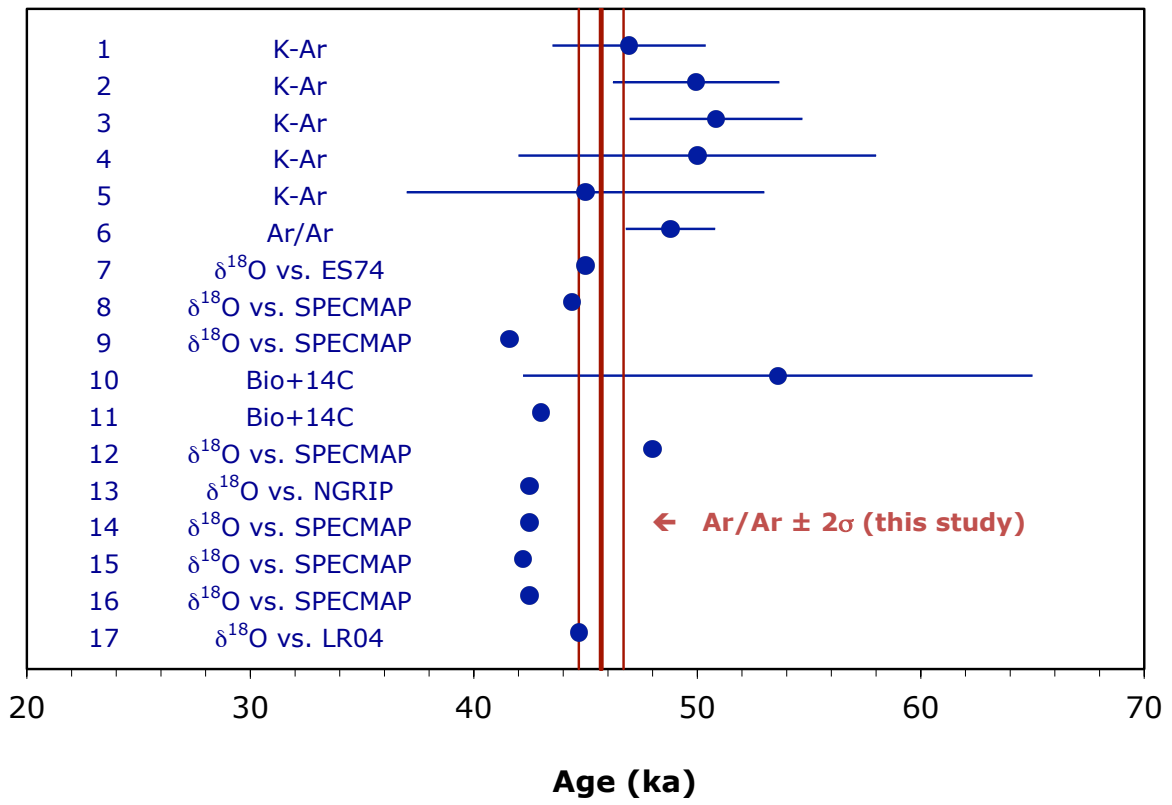
Age (ka)

Sample	Integrated age (ka)	± 2s	N	MSWD	Isochron age (ka)	± 2s	^{40}Ar/^{36}Ar trapped	± 2s	N	MSWD
PAN 06-057	42,78	1,20	14/14	0,76	42,52	2,00	296,12	3,33	14/14	0,81
PAN 06-074	45,42	1,05	29/29	1,44	47,37	1,61	291,04	2,80	29/29	1,13
PAN 06-074bis	44,70	1,05	30/30	0,34	46,20	2,48	291,21	6,36	30/30	0,29
Pooled	44,42	0,63	73/73	0,99	45,65	1,03	292,65	1,97	73/73	0,90

Member	A	B	C	D	E
Facies	pum. fall	pum. flow	weld. eutax.	weld. fines-rich	weld. porphyr
Position	bottom		intermediate		top
Sample/tephra	pan 0720	pan 0721	pan 0722	pan 0723	pan 0731
Composition	Pant.	Pant.	Pant.	Pant.	Trach.
SiO2	69,78	69,72	69,80	70,59	63,07
TiO2	0,59	0,55	0,60	0,60	0,82
Al2O3	9,01	8,51	9,31	9,28	15,66
FeO tot	7,67	8,26	7,74	7,54	5,79
MnO	0,19	0,19	0,11	0,27	0,25
MgO	0,27	0,28	0,26	0,10	0,27
CaO	0,38	0,43	0,40	0,59	0,93
Na2O	6,22	6,21	6,05	6,42	7,05
K2O	4,63	4,71	4,83	4,20	4,72
P2O5	0,01	0,01	0,02	0,04	0,23
F	n.a.	n.a.	n.a.	n.a.	n.a.
Cl	n.a.	n.a.	n.a.	n.a.	n.a.
total	98,76	98,88	99,11	99,63	99,82
L.O.I.	4,45	2,08	1,32	2,00	0,40
peralk. index.	1,69	1,80	1,63	1,63	1,07
Cr ppm	11	17	9	39	20
Ni	12	12	8	0	20
Rb	145	148	140	146	39
Sr	3	2	5	12	66
Y	185	195	139	187	49
Zr	1871	1945	1846	1895	302
Nb	457	480	459	465	73
Ba	289	314	314	290	2159
La	89	95	92	82	57
Ce	312	270	300	278	102

Sample	Member	Olivine Fayalite mole %	Clinopyroxene Na_2O wt%	Alkali feldspar Ab-Or mol % (mean)	Groundmass glass Peralkalinity Index	Accessory minerals
pan 0720	A	88 - 91	1,4	63 - 37	1.1 - 1.7	aenig + qz
pan 0721	B	/	1,0	69 - 31	1.0 - 1.8	aenig + qz
pan 0722	C	/	1.2 - 3.0	66 - 34	1.6 - 1.8	aenig + qz
pan 0723	D	/	2.5 - 9.1	60 - 40	1.3 - 1.5	aenig + qz
pan 0731	E	72 - 86	1.0 - 1.5	70 - 25	0.9 - 1.0	mag + ilm

Member	Thickness*	Petrography, texture and compositional characteristics
A (base)	60-70 cm	Poorly sorted Plinian fall (max. pumice dimension: 6 cm) resting directly on a faintly developed paleosol. Evolved pantellerite composition (peralkalinity index, PI = 1.69), typically low in Sr (3 ppm, Table 1) and extremely enriched in Zr and Nb (1871 and 457 ppm, respectively). Mineral assemblage: Alk-Fsp + cpx + aenig with a distinctively Fe-enriched olivine (Fay = 88-91 mol%, Table 2).
B	40-50 cm	Chaotic, unwelded and fines-rich pumice flow (max. pumice dimension: 5 cm), probably representing the initial stages of column collapse. Slightly more evolved than Member A (PI = 1.80; Zr = 1945 ppm, Nb = 480 ppm).
C	70 cm	Blackish basal vitrophyre (7-10 cm thick) grading into a fiamme-poorer and densely welded facies with a slightly less evolved composition than Members A & B; first pyroclastic density current of the sequence.
D	1 m	Distinctively pistachio-green coloured massive layer; fines-rich and strongly welded. Chemically similar to Member C.
E (top)	50 cm	Brownish porphyritic layer (30 crystal vol.%) dominated by alkali feldspar (up to 4 mm in length). Bulk trachytic composition (PI = 1.07). Except for Sr, incompatible trace elements much less enriched than in the other (pantellerite) facies (e.g., Zr = 302 ppm, Nb = 73, Table S3); distinctly higher Ba content (2159 ppm) probably mirroring some alkali feldspar enrichment due to the depletion in fines during deposition/elutriation Olivine conspicuously less Fe-rich relative to Member A (Fay = 72-86 mol%); amphibole present.

Age (ka)	± 2s	Method	Sample	Site	Source
46,95	3,43	K-Ar	GT	Pantelleria	Cornette et al.
49,95	3,72	K-Ar	GT	Pantelleria	Cornette et al.
50,84	3,87	K-Ar	GT	Pantelleria	Cornette et al.
50,00	8,00	K-Ar	GT	Pantelleria	Mahood and Hildreth (1986)
45,00	8,00	K-Ar	GT	Pantelleria	Mahood and Hildreth (1986)
48,80	2,00	Ar/Ar	GT	Pantelleria	Ton-That (2001)*
45,00	-	$d^{18}O$ vs. ES74	Y-6	Core RC9-191 Ionian S.	Keller et al. (1978)
44.6-44.1	-	$d^{18}O$ vs. SPECMAP	Y-6	Core M25/4-13 Ionian S.	Kraml (1997)
41,60	-	$d^{18}O$ vs. SPECMAP	Y-6	Core M25/4-12 Ionian S.	Kraml (1997)
53,60	11,40	Bio+14C	Y-6	Lesvos (Greece)	Margari et al. (2007)
> 47-43	-	Bio+14C	GT	Pantelleria trough	Anastasakis and Pe-Piper (2006)
~ 48	-	$d^{18}O$ vs. SPECMAP	Y-6	Core M25/4-12 Ionian S.	Anastasakis and Pe-Piper (2006)
42,50	-	$d^{18}O$ vs. NGRIP	Y-6	ODP 160-963A off SW Sicilia	Tamburrino (2008)
42,50	-	$d^{18}O$ vs. SPECMAP	Y-6	ODP 160-963A off SW Sicilia	Tamburrino et al. (2012)
42,20	-	$d^{18}O$ vs. SPECMAP	Y-6	Core M25/4-13 Ionian S.	This study
42,50	-	$d^{18}O$ vs. SPECMAP	Y-6	Core M25/4-12 Ionian S.	This study
44,70	-	$d^{18}O$ vs. LR04	Y-6	ODP 160-963A off SW Sicilia	This study